

Velocity Shear of the Thick Disk from SPM3 Proper Motions at the South Galactic Pole

T. M. Girard, V. I. Korchagin¹, D. I. Casetti-Dinescu² and W. F. van Altena
Yale University, Dept. of Astronomy, P.O. Box 208101, New Haven, CT 06520-8101

girard@astro.yale.edu

C. E. López

Universidad de San Juan, Avenida Benavídez 8175 Oeste, Chimbas, 5413 San Juan, Argentina

D. G. Monet

US Naval Obs., Flagstaff Station, P.O. Box 1149, Flagstaff, AZ 86002

ABSTRACT

The kinematical properties of the Galactic Thick Disk are studied using absolute proper motions from the SPM3 Catalog and 2MASS near-infrared photometry for a sample of ~ 1200 red giants in the direction of the South Galactic Pole. The photometrically-selected sample is dominated by Thick Disk stars, as indicated by the number-density distribution that varies with distance from the Galactic plane as a single-valued exponential over the range $1 < z < 4$ kpc. The inferred scale height of the Thick Disk is 0.783 ± 0.048 kpc. The kinematics of the sample are also consistent with disk-like motion. The U -velocity component is roughly constant, reflecting the Sun's peculiar motion, while a considerable shear is seen in the mean rotational velocity, V . The V -velocity profile's dependence on z is linear, with a gradient of $dV/dz = -30 \pm 3$ km s⁻¹ kpc⁻¹. The velocity dispersions, in both U and V , show a lesser gradient of about 9 ± 3 km s⁻¹ kpc⁻¹. We demonstrate that the derived velocity and velocity-dispersion profiles are consistent with the assumptions of dynamical equilibrium and reasonable models of the overall Galactic potential.

Subject headings: Galaxy: kinematics and dynamics, astrometry

¹also Institute of Physics, Rostov University, Rostov-on-Don 344090, Russia; Isaac Newton Institute of Chile, Rostov-on-Don Branch

²also Astronomical Institute of the Romanian Academy, Str. Cutitul de Argint 5, RO-75212, Bucharest 28, Romania

1. Introduction

The existence of a second, disk-like population in our Galaxy was established on the basis of starcounts by Gilmore & Reid (1983). This population was referred to as a ‘thick disk’, as its derived vertical scale height was greater than that of the previously known Galactic disk. Since then, a considerable number of studies have helped to characterize the Galaxy’s Thick Disk component, in an effort to deduce its origin and better understand its nature. As a result, some of the mean properties of the Thick Disk are now well-established. It consists of old ($\gtrsim 10$ Gyr) stars of intermediate metallicities, ($-1.0 \lesssim [\text{Fe}/\text{H}] \lesssim -0.2$). These stars are kinematically hotter and possess a substantial rotational lag (see e.g., Majewski 1993) relative to old, Thin Disk stars. Most estimates of the Thick-Disk scale height are between 0.8 and 1.2 kpc, and its local normalization is between 2% and 8%, although these two quantities appear to be somewhat anticorrelated (Siegel et al. 2002).

Among the less well-determined parameters of the Thick Disk are its radial scale length and the magnitude of its rotational lag as well as that of its velocity dispersions. Recent determinations of the radial scale length indicate that it is larger than that of the Thin Disk (Robin et al. 1996, Ojha 2001, Chen et al. 2001, Larsen & Humphreys 2003). There are indications that the rotational lag and the velocity dispersions vary with distance from the Galactic plane, (see the review by Majewski 1994). However, the situation is unclear regarding this matter as early studies did not attempt to separate the Thick Disk population from that of the Halo. Thus, the observed variation of the lag with z might be due in part or in whole to the mixture of the two populations. More modern studies (e.g., Majewski 1992, Chiba & Beers 2000, Soubiran et al. 2003) explicitly separate the two populations by metallicity when determining the kinematical parameters. Unfortunately, these studies do not agree. For instance, Soubiran et al. (2003) find no significant kinematic gradients, although their study reaches only to $z = 0.8$ kpc, while Majewski (1992), whose deep proper-motion survey samples the Galaxy out to $z \sim 6$ kpc, does detect significant gradients, with that of the rotational lag being $-21 \text{ km s}^{-1} \text{ kpc}^{-1}$. Chiba & Beers (2000) find an even steeper gradient for the lag, $-30 \text{ km s}^{-1} \text{ kpc}^{-1}$. It is important to note that the Chiba & Beers study covers a large portion of the sky, unlike most studies that are made only toward the Galactic poles. It also makes use of a large sample of stars (~ 1200) with known metallicities, proper motions, radial velocities, and distance estimates. We regard this study as a significant step forward in understanding both the Thick Disk and the inner Halo – its primary limitation being that it only probes the Galaxy to $z \lesssim 2$ kpc. Lastly, a very recent study (Allende Prieto et al. 2006) that uses SDSS photometric distances and radial velocities alone, finds a rotational lag gradient of $-16 \text{ km s}^{-1} \text{ kpc}^{-1}$, between $z = 1$ and 3 kpc.

From this brief summary, it is obvious that the kinematics of the Thick Disk are still

poorly known. We note the following case, for example, in which a proper interpretation of the data hinges upon better knowledge of the Thick-Disk rotational z -gradient. Recently, Gilmore et al. (2002) (see also Wyse et al. 2006) presented radial-velocity results of some 2000 faint F/G stars observed in two lines of sight chosen specifically to probe Galactic rotation. They found that many of these stars, residing up to 5 kpc from the Galactic plane, rotate at $\sim 100 \text{ km s}^{-1}$, i.e., with a lag of $\sim -120 \text{ km s}^{-1}$. Their interpretation, which assumes a single-valued lag for the Thick Disk of -35 km s^{-1} , is that these high-lag stars are debris from a disrupted satellite that merged with the Galaxy in a significant accretion event. Alternatively, one might also explain these observations as the natural result of a Thick Disk whose lag varies substantially with z , such as has been observed by Chiba & Beers (2000).

Finally, we note that while previous studies have attempted to determine the variation of the Thick Disk’s rotational lag and velocity dispersions as functions of z , there have been no attempts to examine the resulting velocity and dispersion profiles for self-consistency within the context of the expected dynamical equilibrium of a disk system, a question first posed by Murray (1986). It is the purpose of the present study to determine the kinematical properties of the Thick Disk as functions of z out to ~ 4 kpc, and to investigate the dynamical equilibrium of this system. The sample used in our analysis consists of ~ 1200 Thick-Disk red giants at the South Galactic Pole. These are selected photometrically from 2MASS, and have absolute proper motions taken from the SPM3 Catalog (Girard et al. 2004).

In the following section, we provide details of the sample selection. In Section 3, we describe the methods used to determine first the observed and then the intrinsic spatial and kinematical parameters of the Thick Disk. Section 4 contains our equilibrium analysis of the resulting Thick Disk parameters, followed by a general discussion of our findings in Section 5. Our main results are summarized in Section 6.

2. Sample Selection

The most recent release by the Yale/San Juan Southern Proper Motion program is the SPM3 Catalog (Girard et al. 2004). This catalog of absolute proper motions of over 10 million stars is complete to $V = 17.5$ and covers an irregular area between declinations -20° and -45° , excluding the Galactic plane. We combine SPM3 proper motions with 2MASS photometry for a sample of bright, high-latitude red giants, allowing us to examine the transverse velocity structure of the Thick Disk.

The sample is selected from ~ 1700 stars in the SPM3 Catalog within 15 degrees of

the South Galactic Pole (SGP), and within the region of the 2MASS J, K color-magnitude diagram shown in Figure 1. The sloping cutoff limit at the faint end is meant to assure that only the most nearby ($d < 63$ pc) dwarfs might contaminate the sample. The local density of low-mass dwarfs was tabulated by Holmberg & Flynn (2000, see their Table 1), and is roughly $0.025 M_{\odot}/\text{pc}^3$ over the color range of our sample. Thus, within the corresponding volume of our sample cone, within 63 parsecs for dwarf-star magnitudes, we expect on the order of several hundred such stars within our sample volume. As will be seen in Section 3.1, if we calculate stellar velocities assuming red-giant distance moduli for the sample stars, it is relatively easy to choose a conservative velocity cutoff that cleans the sample of these kinematically obvious nearby dwarfs. When done, this results in the reduction of the sample size to ~ 1200 stars.

Another possible source of contamination, that from AGB-stars, is negligible. Jackson et al. (2002) find that the distribution of AGB-stars in the direction perpendicular to the Galactic plane is described by an exponential function with a vertical scale height of 0.3 kpc and a density of about 150 kpc^{-3} in the solar neighborhood, indicating that not more than a few AGB-stars should be in our sample.

The color range of the sample was chosen to preferentially select intermediate-metallicity stars (Thick Disk) as opposed to metal-poor ones (Halo). As will be seen in Section 3.3, the fraction of Halo stars in our sample can be estimated from the observed number-density profile. This fraction turns out to be small, about 8 percent, and its presence is included in the modeling of the sample’s kinematics.

We note that the areal coverage of the sample does not fill the entire 15-degree circular cone centered on the SGP. The southernmost boundary of the SPM3 Catalog limits the sample to roughly 70 percent of this volume. Nonetheless, within this cone of irregular cross-section, our sample of red giants is expected to be volume-complete from $z = 0.5$ to 3 kpc.

One final characteristic of our sample warrants discussion. Monte-Carlo simulation of the observed data will be used to deduce the sample’s intrinsic kinematic properties. This method depends on the proper-motion uncertainties for these stars being well-determined. Individual proper-motion uncertainties are estimated for all stars in the SPM3 Catalog based on proper-motion differences between different image systems and exposures. As is often the case, these internal uncertainty values may underestimate the true uncertainties, on average. In order to “calibrate” the SPM3 proper-motion uncertainty estimates, we select all stars in the SPM3 Catalog that are also Hipparcos stars and examine the differences in the SPM3 and Hipparcos proper-motion determinations. The number of such stars is 10,900 and the dispersion of the differences is 3.75 mas yr^{-1} . The Hipparcos measuring

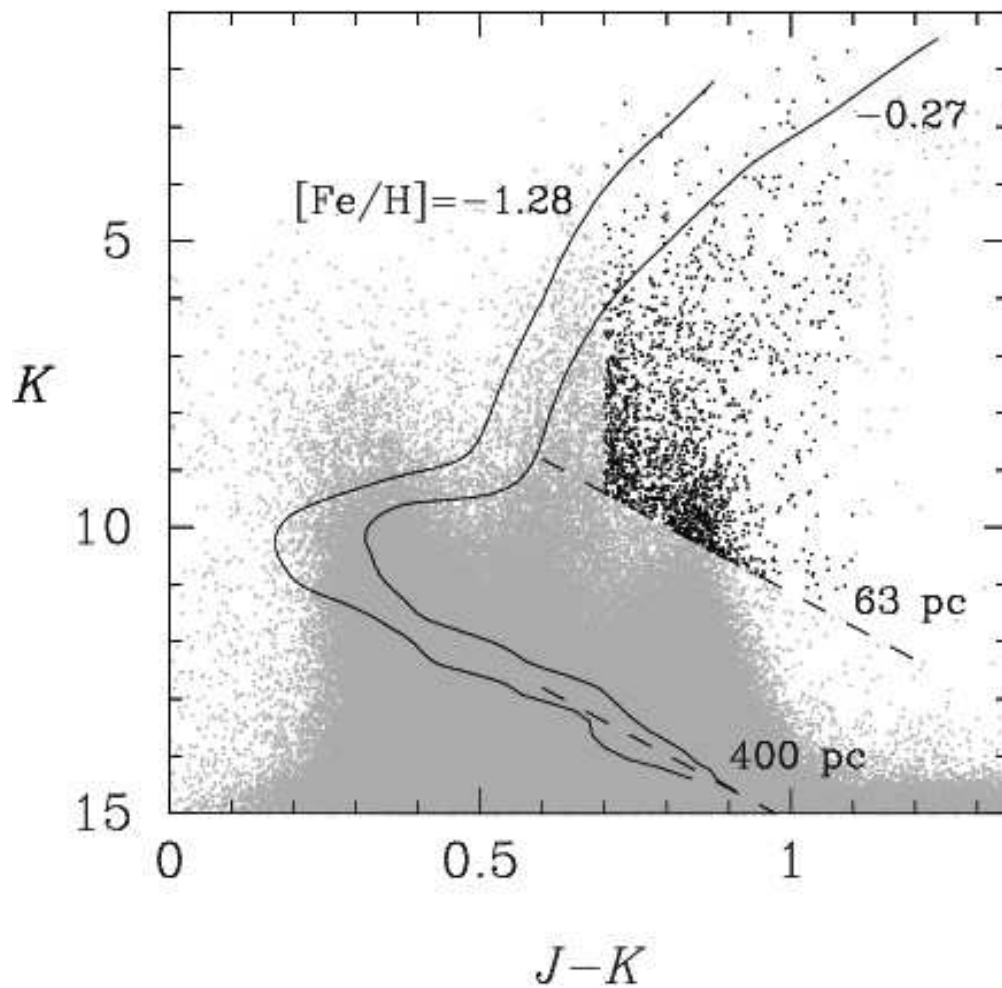


Fig. 1.— Color-magnitude selection of the sample, based on 2MASS JK photometry. The sample consists of stars within 15 degrees of the SGP, with $0.70 < J - K < 1.10$, and with K -magnitude brighter than the sloping limit shown. For comparison, 5-Gyr Yale-Yonsei theoretical isochrones (Yi et al. 2003) for two different metallicities are overlaid, placed at an arbitrary distance of 400 pc. The sloping cutoff used to select our sample corresponds roughly to the main sequence at a distance of 63 pc.

errors are approximately 1 mas yr^{-1} , thus, the mean SPM3 proper-motion error for these stars is 3.61 mas yr^{-1} . The trimmed mean uncertainty estimates from the SPM3, for these Hipparcos stars, is 3.12 mas yr^{-1} . Therefore, adjustment by a factor of 1.16 is in order and should be applied to the SPM3 internal uncertainty estimates for these bright, well-measured stars. In fact, our SGP sample stars are among the best-measured in the SPM3 Catalog, being slightly fainter than the Hipparcos stars and at the optimal magnitude range for the SPM plate material. The trimmed mean, SPM3-estimated proper-motion uncertainty for the SGP sample is 2.58 mas yr^{-1} . We adopt 1.16 times this value, 3.0 mas yr^{-1} , as the actual proper-motion uncertainty for our SGP red-giant sample.

3. Proper-Motion/Photometry Analysis

Our goal is to derive the tangential velocity distribution of the Thick Disk as a function of distance from the Galactic plane, z , based on our proper-motion sample. Details of how this is accomplished are given below, but the general procedure is as follows: Individual stellar distances are estimated photometrically, using 2MASS K apparent magnitudes and an adopted absolute-magnitude calibration. At a given distance, a star’s (U, V) velocity components are then simply computed from its measured proper motion, (μ_U, μ_V) . The average velocity and velocity dispersion of the sample, as a function of z , is then determined.

Uncertainties in the derived distances will affect the sample’s “observed” density, velocity, and velocity-dispersion profiles, altering them from their actual, intrinsic forms. There are several distinct mechanisms associated with the sample selection and distance estimation that combine to produce a bias in the observed profiles. Chief among these is the convolution of the distance errors with the sharply rising frequency distribution of stars as a function of z . It is essential that compensation be made for all these effects, as well as those caused by uncertainties in the measured proper motions. We do so by modeling the effects on simulated data, as described in Section 3.2. The conversion from measured quantities (apparent magnitudes, proper motions) to stellar parameters (distance, velocity) is described first.

3.1. Observed Sample

Our sample has been cut from a portion of the J, K color-magnitude diagram to preferentially select red giants at distances of 0.5 to 4 kpc. The sample is dominated by Thick-Disk, intermediate-metallicity giants, so the expected absolute magnitudes of these stars can be estimated as a function of color. Yale isochrones (Yi et al. 2003) have been used, and

convolved with an adopted Thick-Disk metallicity distribution to yield absolute M_K magnitude distributions as a function of $J - K$ color bin. The assumed metallicity distribution is taken from Wyse & Gilmore (1995), (the intermediate component of their Figure 16). The resulting absolute-magnitude distributions that we adopt are shown in Figure 2.

For a particular star with known apparent magnitude K , the range in absolute magnitude corresponds to a range in derived distance. We distribute each star over a range of distance by artificially partitioning the star into 100 subunits and randomly drawing a value of M_K for each subunit, utilizing the absolute-magnitude distribution as a probability distribution.

Velocity components are derived for each subunit, thus distributing the star in velocity space as well. Note that the uncertainties in the extinction-corrected values of K and $J - K$ are negligible relative to the width of the absolute-magnitude distributions. In this manner, the absolute proper motions as a function of apparent magnitude, shown in Figure 3, are converted to velocities as a function of z , shown in Figure 4. Obviously, a substantial fraction of the derived velocities are not physically meaningful. Nearby dwarfs misinterpreted as giants are assumed too distant and erroneously given large velocities. The large increase in proper-motion dispersion beyond $K = 9$ in Figure 3 is precisely due to the incursion of nearby dwarfs into the sample. The velocities calculated for these stars, under the assumption that they are giants, fall well outside the trend of the Thick Disk giants seen in Figure 4, often beyond the plotted limits of the velocity axis, in fact. To minimize this source of contamination, we cut those (subunits of) stars which have velocities greater than the local escape velocity, i.e., in excess of 550 km s^{-1} relative to an assumed LSR velocity of $V = -220 \text{ km s}^{-1}$. This trimming effectively decreases the size of our SGP sample from 1700 stars to roughly 1200 stars.

An alternative to velocity trimming of the sample would be to use the reduced proper motion diagram to separate giants and dwarfs. The reduced proper motion is a kinematic estimate of absolute magnitude and is given by

$$H_K = K + 5 \log |\mu| + 5,$$

where $|\mu|$ is the total magnitude of the star's proper motion, in arcsec yr^{-1} . In Figure 5, the reduced proper motion in K -band is plotted versus $J - K$ for our SGP sample. The result of the subunit velocity trimming we have adopted is illustrated by the different symbols in the figure. Those stars for which 95% or more of their subunits pass the velocity trimming are shown as solid symbols. These, presumably, are the desired giants. Stars for which 5% or fewer of their subunits pass the velocity trimming are shown as open circles. These are more nearby dwarfs. A smaller number of stars, shown as crosses, have between 5% and 95% of their subunits that satisfy the velocity cut. These lie almost exclusively in the less

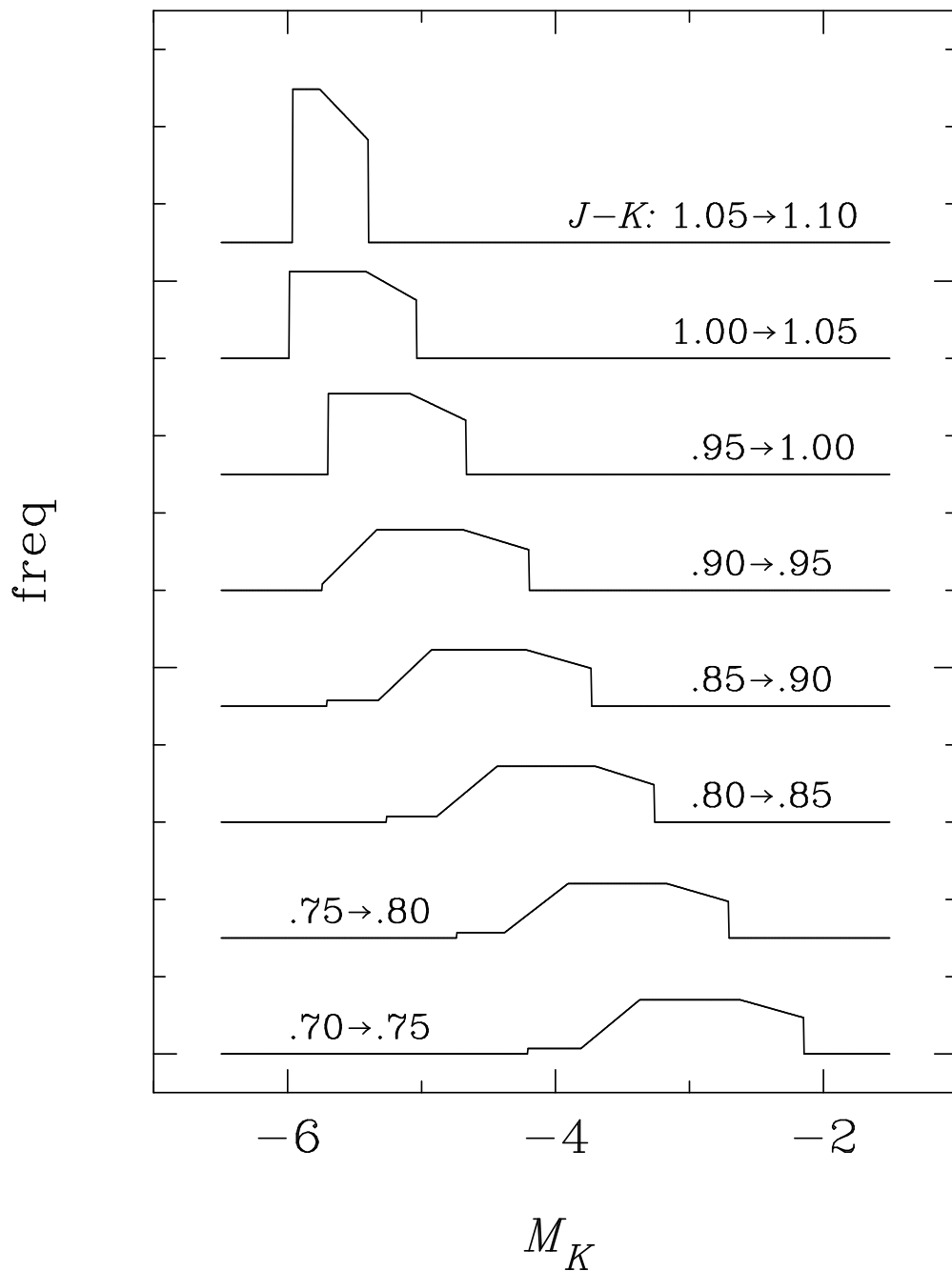


Fig. 2.— Assumed red-giant absolute magnitude distribution, by color bin, used in the photometric distance determinations. These distributions were constructed by combining the Thick-Disk metallicity distribution measured by Wyse & Gilmore (1995) with Yale-Yonsei theoretical isochrones, (Yi et al. 2003).

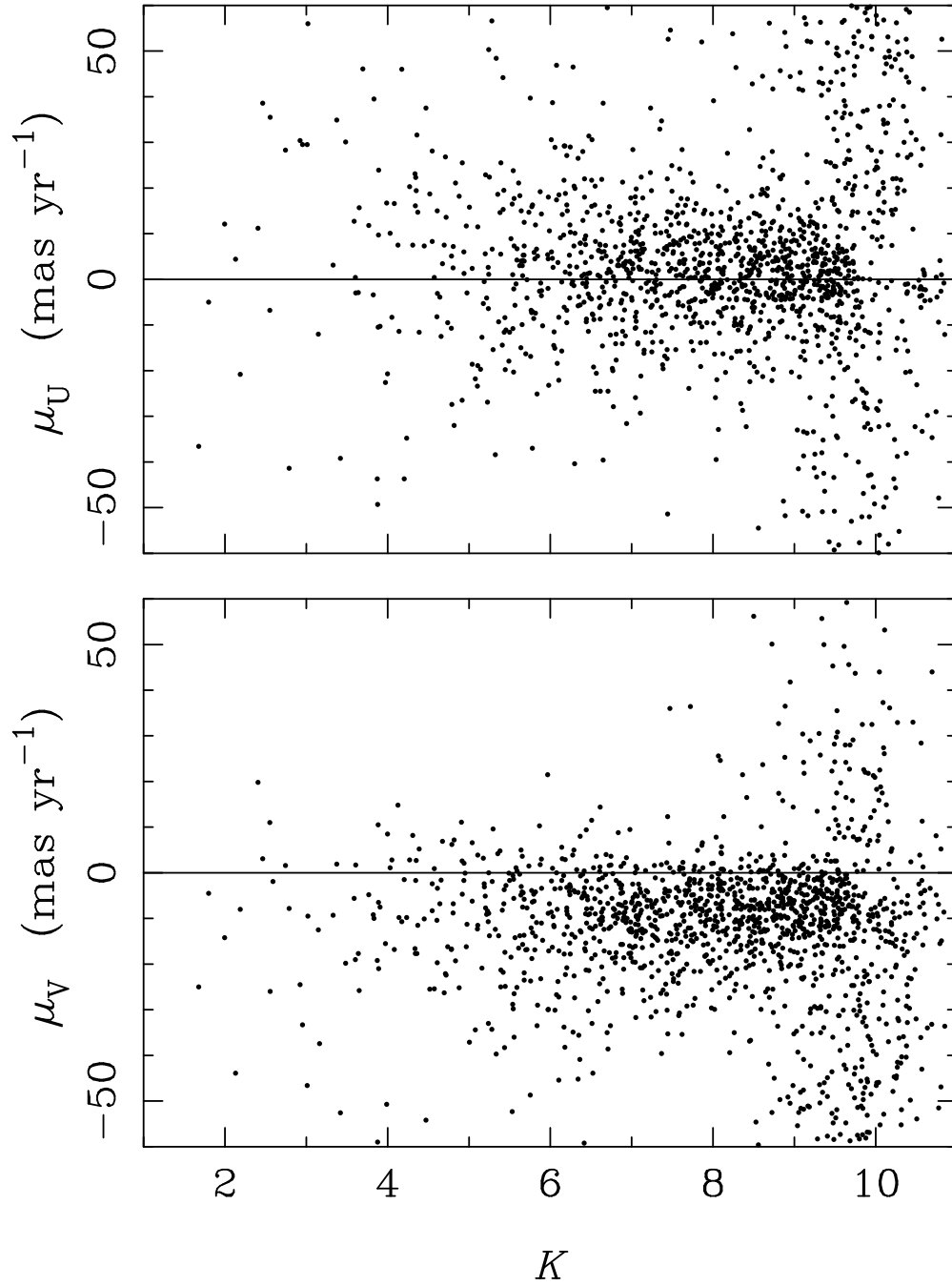


Fig. 3.— Absolute proper motions as a function of magnitude for the photometrically selected red-giant sample. U is positive outward from the Galactic center, and V is in the direction of Galactic rotation.

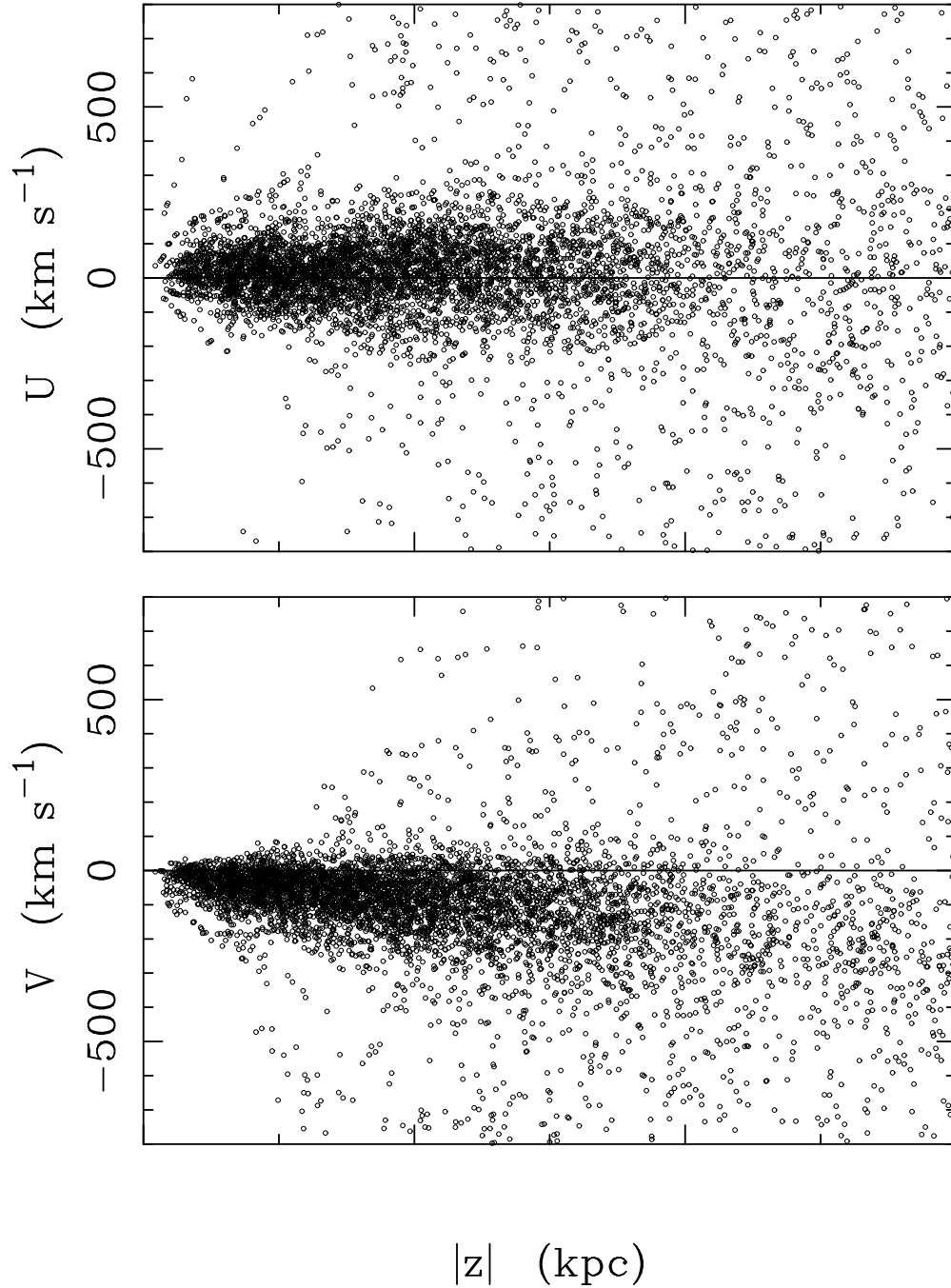


Fig. 4.— Tangential velocities as a function of distance from the Galactic plane, z . Each star is assigned a distribution of 100 absolute magnitudes, randomly drawn from the luminosity functions given in Figure 2. Each point in the plot represents one of the 100 such “subunits” per star.

populated region between giants and dwarfs in the diagram. Thus, the subunit velocity trimming produces a giant/dwarf segregation that is virtually identical to that which would have resulted from a simple cut by reduced proper motion. The subunit velocity trimming provides a means of partially including borderline stars in the sample, but only those subunits for which the randomly selected absolute magnitudes lead to reasonable velocities.

After velocity trimming, the distributions of star density, velocity, and velocity-dispersion are computed as functions of z . The resulting distributions are shown in Figure 6. These profiles are constructed by sorting the subunits in z and binning them, 100 subunits per bin. Thus, each point in Figure 6 has the weight of one star, although in general a point will have contributions from numerous stars, effectively smoothing the data. The average (median-based) velocity and velocity dispersion of each bin is estimated using the probability-plot method, (Hamaker 1978), using the inner 80 percent of each bin’s velocity distribution. This leads to a more robust dispersion estimate, one that is less influenced by outliers - whether they be actual mismeasures or a small fraction of contaminating stars from a kinematically hotter population, i.e., Halo stars.

The observed log-density profile in Figure 6 indicates a nearly linear trend in the range 1 to 4 kpc. Based on the imposed faint-limit cutoff of our sample and the bright limit of the SPM3 Catalog, combined with the assumed absolute-magnitude distributions, we estimate that our red-giant sample is expected to be complete from approximately $z = 0.5$ to 3 kpc. There are appreciable deviations from otherwise smooth trends in the range of 0.5 to 1 kpc in all of the observed profiles. These possibly show the presence of Thin Disk giants over this range and/or small-number fluctuations, keeping in mind that the volume density of stars is proportional to the counts but inversely proportional to the square of the distance for our sampling cone. On the other hand, in the range $z = 3$ to 4 kpc, while some incompleteness is expected, the various observed profiles continue their trends across this region. Thus, we choose to concentrate our analysis on the range $z = 1$ to 4 kpc. It is over this range that we will attempt to parameterize the underlying density, velocity and dispersion profiles of our sample.

3.2. Simulated Samples

As stated earlier, a correction must be made to the observed profiles to compensate for systematic effects caused by measurement uncertainties. The strategy we employ is to characterize the distance and proper-motion uncertainties in detail and apply them to simulated data sets, in a Monte Carlo fashion. The generated samples are assigned artificial errors in distance (via the absolute magnitudes) and in proper motion, consistent with the

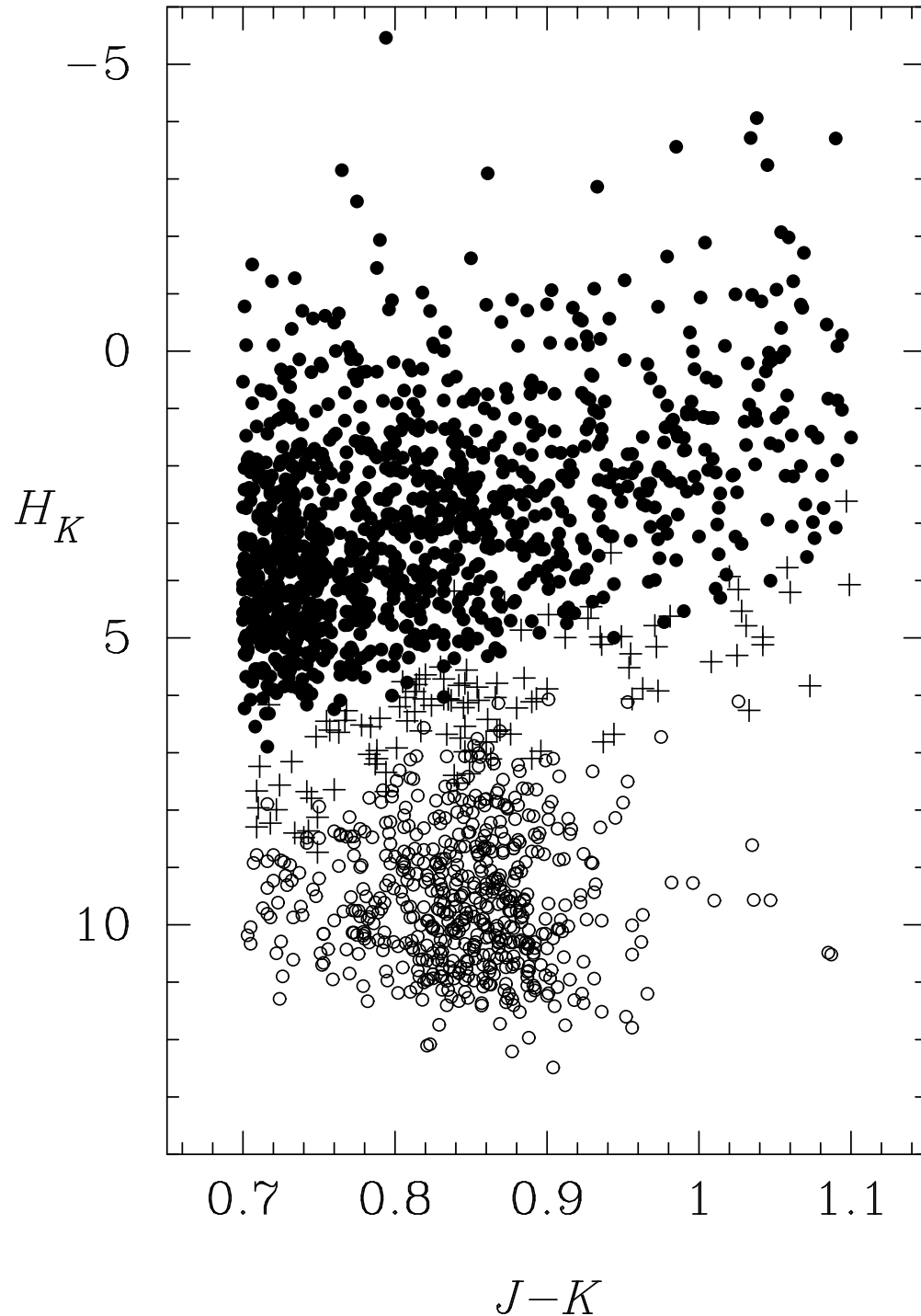


Fig. 5.— Reduced proper motion diagram for the SGP sample. Symbols represent delimitation in the fraction of each star’s subunits that survive the velocity trimming, i.e. total velocity relative to that of the LSR less than 550 km s^{-1} . Solid dots are stars with 95% or more subunits passing the trimming. Open circles are stars with 5% or fewer of their subunits passing the cut. Crosses represent the remaining stars whose subunits survive the velocity trimming with a frequency that falls between these two values.

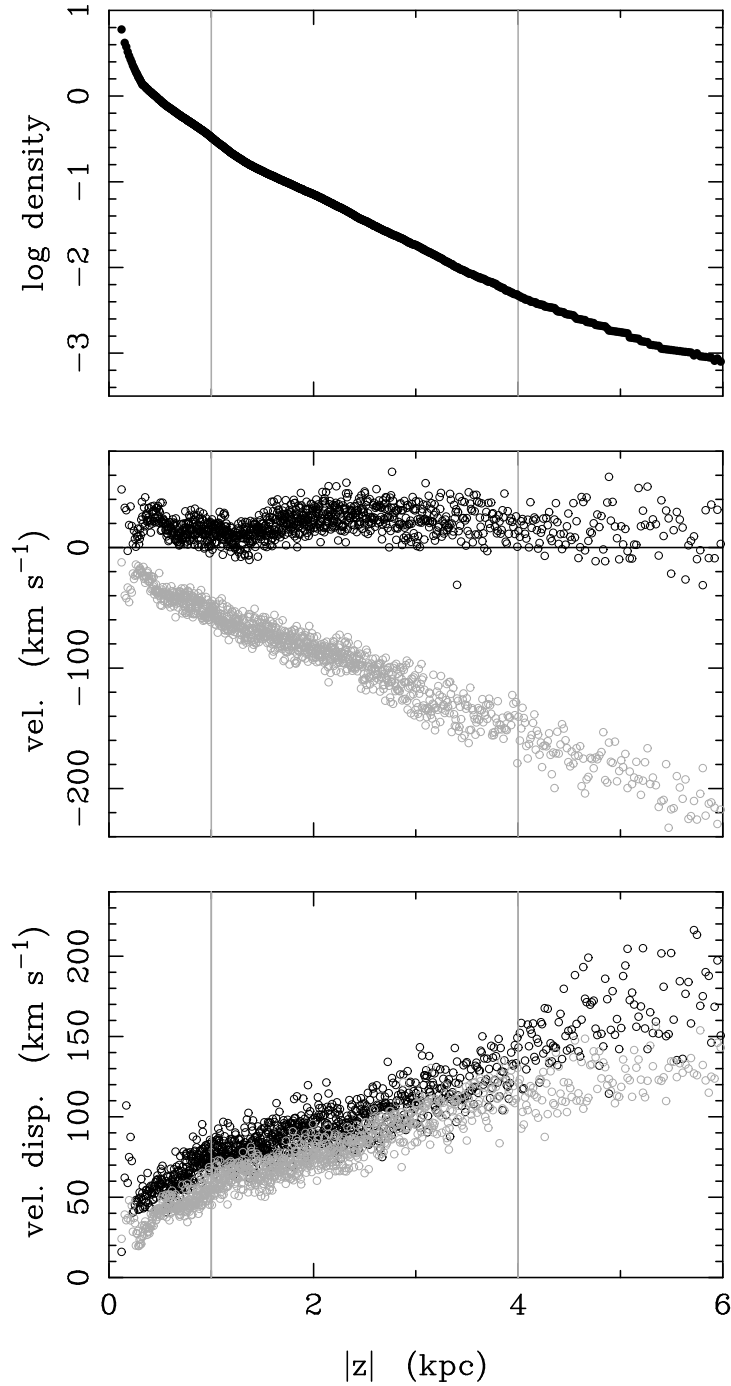


Fig. 6.— Stellar density, velocity, and velocity-dispersion as a function of z for the observed sample of ~ 1200 red giants. Star “subunits” are sorted in z and then binned in groups of 100 to calculate the total density, mean velocity, and dispersion in each bin. In the lower two panels, dark symbols are for the U velocities and lighter symbols are for the V velocities.

uncertainty distributions of the actual SGP sample. The simulated data sets are then used to determine the transformation between the intrinsic and “observed” density, velocity, and velocity-dispersion profiles. This transformation, when inverted, can then be used to determine the intrinsic parameters of our SGP sample from its observed profiles shown in Figure 6. Once the intrinsic parameters are determined, their uncertainties can be estimated in a standard Monte Carlo approach. That is, a number of simulations with these same intrinsic parameters is run, and the “observed” profiles are generated and then used to estimate the input intrinsic parameters. The distribution of derived intrinsic parameters about the known input values provides an estimate of their uncertainties.

The model we construct for our simulations consists of two components, a planar component having an exponential density distribution in z which we identify with the Thick Disk, and a spherical component with a power-law density distribution in Galactocentric radius and which we identify with the Inner Halo. The spatio-kinematic characteristics of the Halo component are assumed known, and will be taken from the literature, whereas those of the Thick Disk component are the subject of this investigation and are to be determined.

The power-law index for the Halo density is assumed to be -3.5, (Zinn 1985). A somewhat less negative index might be appropriate for the inner Halo, but at the adopted Galactocentric distance of the sun, assumed to be 8 kpc, the Halo density changes very little over the $z = 1$ to 4 kpc region of interest for any reasonable choice of index. Thus, the precise value of the power-law index is not critical. The velocity and velocity dispersion for the Halo component are assumed to be independent of z . Values are taken from Table 2 of Chiba and Beers (2000), using mean parameters of their more distant samples with $[\text{Fe}/\text{H}] \lesssim -1.5$. The adopted Halo velocity parameters are: $U_H = 16 \text{ km s}^{-1}$, $V_H = -180 \text{ km s}^{-1}$, $\sigma_{UH} = 150 \text{ km s}^{-1}$, $\sigma_{VH} = 120 \text{ km s}^{-1}$. The only free parameter associated with the Halo component is the fraction of Halo stars, f_H , which is to be determined for our SGP sample.

The simulated Thick Disk component is parameterized as follows. The number-density distribution is assumed a pure exponential, with scale height $h_{z_{thick}}$. The velocity and velocity dispersion in U and V are expressed as linear functions of z . It is not that we have theoretical reasons to suspect linear relations, but simply that the observed velocity and dispersion profiles show an apparent linear trend over the region of interest and we do not feel that the data would allow us to deduce terms higher than first-order. Thus, it is assumed that the intrinsic velocity and dispersion profiles can be adequately described by linear functions

$$\begin{aligned} U &= U_o + U'|z|, \\ V &= V_o + V'|z|, \\ \sigma_U &= \sigma_{U_o} + \sigma'_U|z|, \end{aligned}$$

$$\sigma_V = \sigma_{V_o} + \sigma'_V |z|.$$

A simulation is characterized by the ten parameters f_H , $h_{z_{thick}}$, U_o , U' , V_o , V' , σ_{U_o} , $\sigma'_{U'}$, σ_{V_o} , $\sigma'_{V'}$. The desired number of Halo giants is generated, falling within a 15-degree cone at the SGP and randomly selected from the power-law distribution in Galactocentric radius, r . Thick Disk giants are similarly generated within the cone and distributed with an exponential falloff in z , with scale height $h_{z_{thick}}$. Each star is given a $J - K$ color drawn from a distribution that follows the colors of the actual SGP sample. Based on the color, an absolute magnitude M_K is assigned, drawn from the appropriate magnitude distribution of Figure 2. A slightly different set of low-metallicity M_K distributions is employed for the Halo stars. Once the distance and absolute magnitude are assigned, the apparent magnitude is calculated and checked to see if it falls above the sloping apparent-magnitude cutoff used to define the SGP sample. If so, the star is retained and given randomly selected U and V velocities, drawn from the appropriate velocity- z relations for that stellar component. Gaussian distributions about the mean velocity trends are assumed, with dispersions given as a function of z as specified by the input parameters. The combination of U and V with z , and Galactic latitude, specify the star’s precise proper motion, (μ_U, μ_V) . The “observed” proper motion is generated by adding a random deviate chosen from a Gaussian distribution whose standard deviation is 3.0 mas yr^{-1} , the measuring uncertainty determined for our SGP sample. Thick Disk and Halo giants are accumulated in the desired ratio, based on f_H , until the sample consists of 1160 stars, the approximate size of the velocity-trimmed SGP sample.

After the simulated sample is generated, it is passed through the same reduction procedure that was applied to the actual SGP sample. Note that absolute magnitudes are derived based only on the intermediate-metallicity curves of Figure 2, as at this point the distinction between Thick Disk and Halo stars is intentionally discarded. This is not too crude of an approximation as the magnitude distributions for the low- and intermediate-metallicity giants do not vary greatly, and the fraction of Halo stars turns out to be small. More importantly, any systematic effect caused by this approximation will also be present in the actual SGP sample’s reduction and should, therefore, be mimicked here. Density, velocity, and dispersion profiles are constructed for each simulation in the same way as was done for the SGP sample. A representative example is shown in Figure 7, for a simulation with input parameters very near the final best-fit values for the SGP sample.

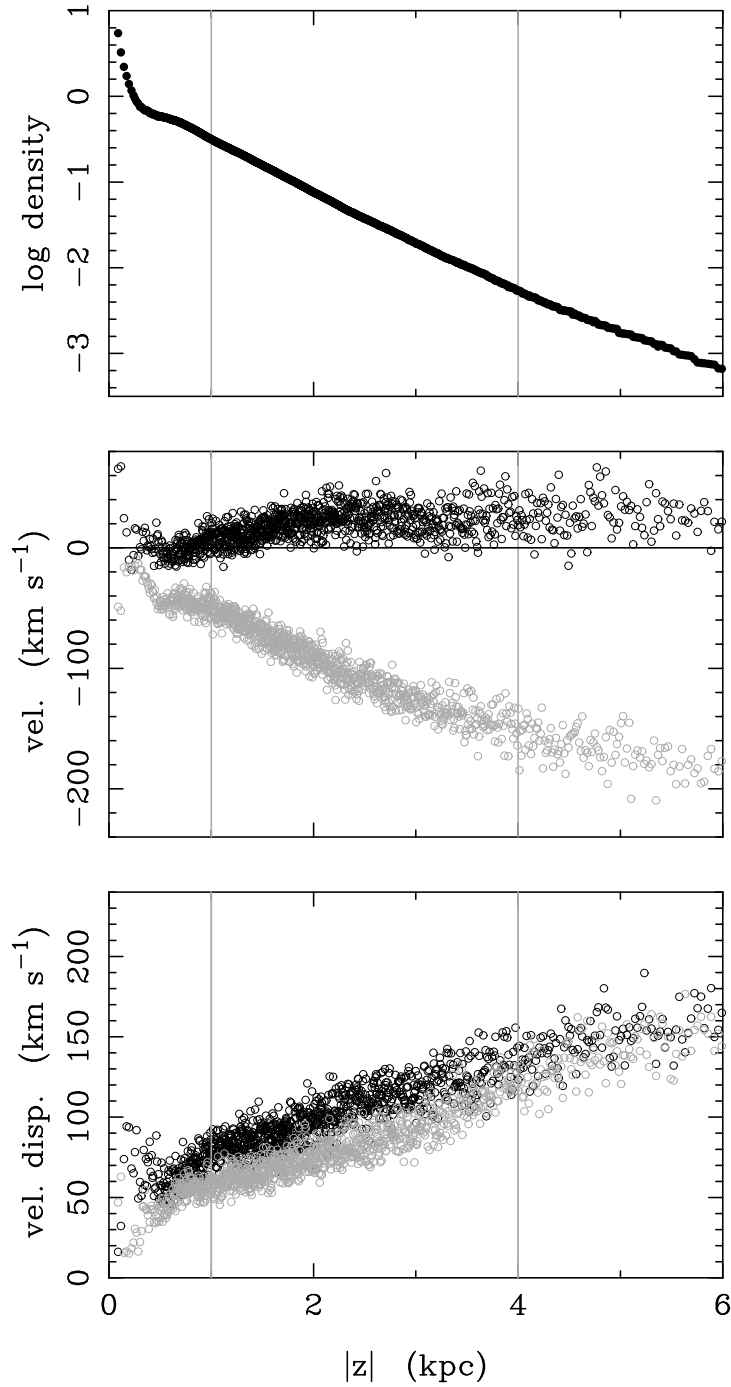


Fig. 7.— Stellar density, velocity, and velocity-dispersion as a function of z for a single simulated sample. The construction of the distributions and the plotting symbols are the same as used for the observed sample, shown in Figure 6. The spatio-kinematic input parameters of this simulation are very near those of the best-fit determination given in Section 3.3

3.3. Intrinsic Parameter Estimation

The primary purpose of the simulations is to provide a means of determining the relationship between the ten input model parameters and the simulated “observed” density, velocity, and dispersion profiles. The various parameters are evaluated as follows.

The value of the Halo fraction influences all of the profiles in Figure 7. However, the density profile provides the most direct measure of this parameter. The slope and curvature of the log-density plot depends on the combination of $h_{z_{thick}}$ and f_H . We characterize the output profile by fitting a quadratic polynomial to the log-density as a function of z , from $z = 1$ to 4 kpc,

$$\log(\rho) = a_0 + a_1|z| + a_2|z|^2.$$

The values of a_1 and a_2 will be functions of the input parameters $h_{z_{thick}}$ and f_H . This functional dependence is determined by generating simulations on a 2-d grid that spans a suitable range of the input parameters, (i.e., $0.0 < f_H < 0.4, 0.6 < h_{z_{thick}} < 0.9$ kpc). At each grid point a series of 25 simulations was performed and means of the best-fit values of a_0 , a_1 , and a_2 determined. Linear fits of a_1 and a_2 as functions of the input parameters were then found by least-squares,

$$a_1 = -3.74 + 2.87h_{z_{thick}} - 0.15f_H$$

$$a_2 = 0.30 - 0.367h_{z_{thick}} + 0.18f_H$$

where $h_{z_{thick}}$ is in kpc. The above can be inverted to provide the desired means of estimating the intrinsic parameters, $h_{z_{thick}}$ and f_H , given a measurement of the observed density-profile parameters, a_1 and a_2 .

For our SGP sample, the least-squares-determined values of a_1 and a_2 are -1.51 and 0.027, respectively. Substituting these into the above relations and solving yields $f_H = 0.08$ and $h_{z_{thick}} = 0.783$ kpc. Uncertainty estimates for these and the other intrinsic parameters will be presented in the following subsection.

With the Halo fraction determined, and found to be relatively low, we now proceed to modeling of the U and V velocity profiles. The two components are treated separately and are assumed to be independent of one another. Again, simulations are carried out over a grid of values, in this case two grids, varying U_o and U' over an appropriate range of values for one grid, and varying V_o and V' in the other. Least-squares fits of the resulting U and V profiles are made, this time using linear functions of z , fitting over the same 1 to 4 kpc region. This yields a grid of “observed” values of intercept and slope for the simulated profiles. The mapping from intrinsic velocity-profile parameters to observed ones is made by least-squares

fitting. The resulting relationships, in the two components, are

$$\begin{aligned}
 U_o &= -0.696 + 1.18\hat{U}_o - 0.373\hat{U}' \\
 U' &= -1.28 + 1.20\hat{U}' \\
 V_o &= -10.7 + 1.15\hat{V}_o - 0.316\hat{V}' \\
 V' &= 8.46 + 1.21\hat{V}'
 \end{aligned}$$

where parameters marked with a $\hat{}$ indicate observed quantities as opposed to intrinsic ones.

The observed profile parameters for the actual SGP sample are $\hat{U}_o = 9.63 \text{ km s}^{-1}$, $\hat{U}' = 5.12 \text{ km s}^{-1} \text{ kpc}^{-1}$, $\hat{V}_o = -21.8 \text{ km s}^{-1}$, $\hat{V}' = -32.1 \text{ km s}^{-1} \text{ kpc}^{-1}$. From the above relations, these correspond to best-estimate values for the sample's intrinsic velocity parameters of $U_o = 8.7 \text{ km s}^{-1}$, $U' = 4.8 \text{ km s}^{-1} \text{ kpc}^{-1}$, $V_o = -25.8 \text{ km s}^{-1}$, $V' = -30.3 \text{ km s}^{-1} \text{ kpc}^{-1}$.

A similar treatment of the velocity dispersions is made. Linear descriptions of the observed and intrinsic dispersion profiles are used. As will be seen in Section 4.2, a strictly linear dependence on z of both the velocity and velocity-dispersion profiles is not consistent with the assumed condition of equilibrium for our sample, given a reasonable distribution for the underlying potential. However, given the quality of the data over the applicable range in z , descriptions of the profiles that include higher than first-order terms are not warranted. With this in mind, the derived relationship between observed and intrinsic profile linear parameters is

$$\begin{aligned}
 \sigma_{U_o} &= 26.1 + 1.16\hat{\sigma}_{U_o} - 0.853\hat{\sigma}'_U \\
 \sigma'_U &= -22.2 + 1.62\hat{\sigma}'_U \\
 \sigma_{V_o} &= 26.1 + 1.16\hat{\sigma}_{V_o} - 0.976\hat{\sigma}'_V \\
 \sigma'_V &= -24.6 + 1.75\hat{\sigma}'_V
 \end{aligned}$$

where again a variable with a $\hat{}$ indicates an observed quantity.

The observed dispersion profile parameters of the SGP sample are $\hat{\sigma}_{U_o} = 55.7 \text{ km s}^{-1}$, $\hat{\sigma}'_U = 18.3 \text{ km s}^{-1} \text{ kpc}^{-1}$, $\hat{\sigma}_{V_o} = 36.5 \text{ km s}^{-1}$, $\hat{\sigma}'_V = 20.0 \text{ km s}^{-1} \text{ kpc}^{-1}$. These correspond to the following best-estimate values for the sample's intrinsic velocity-dispersion parameters: $\sigma_{U_o} = 74.8 \text{ km s}^{-1}$, $\sigma'_U = 7.5 \text{ km s}^{-1} \text{ kpc}^{-1}$, $\sigma_{V_o} = 48.7 \text{ km s}^{-1}$, $\sigma'_V = 10.5 \text{ km s}^{-1} \text{ kpc}^{-1}$.

We now estimate the uncertainties in all of the derived intrinsic parameters.

3.4. Parameter Uncertainties

Uncertainties in the derived values of the intrinsic Thick Disk parameters are estimated using Monte Carlo techniques. A series of 100 simulations is performed, using our best-estimate values for the intrinsic parameters. Each simulated data set is then reduced through the same series of steps as was the actual SGP sample. That is, every star is represented by 100 subunits, each with its own photometric distance estimate; the subunits are binned by z ; density, velocity and dispersion are calculated for each bin, the latter two using probability-plot methods; the resulting “observed” distributions are fit over the range $1 < z < 4$ kpc, using quadratic (density) and linear (velocity and dispersion) functions of z ; then these profile fitting parameters are used to determine estimates of the ten intrinsic parameters, as just described. The distribution of the derived values for each intrinsic parameter provides an estimate of the uncertainty in that parameter.

The resulting distributions are found to be roughly normal, for all ten intrinsic parameters. Adopting the standard deviation of each parameter’s distribution as a one-sigma uncertainty in its determination leads to the following final estimates for the intrinsic Thick Disk parameters:

$$\begin{aligned}
 f_H &= 0.080 \pm 0.056 \\
 h_{z_{thick}} &= 0.783 \pm 0.048 \text{ kpc} \\
 U|_{z=2.2} &= 19.1 \pm 2.7 \text{ km s}^{-1}, U' = 4.8 \pm 2.9 \text{ km s}^{-1} \text{ kpc}^{-1} \\
 V|_{z=2.2} &= -91.6 \pm 1.9 \text{ km s}^{-1}, V' = -30.3 \pm 3.2 \text{ km s}^{-1} \text{ kpc}^{-1} \\
 \sigma_U|_{z=2.2} &= 91.1 \pm 2.9 \text{ km s}^{-1}, \sigma'_U = 7.5 \pm 3.1 \text{ km s}^{-1} \text{ kpc}^{-1} \\
 \sigma_V|_{z=2.2} &= 71.5 \pm 1.9 \text{ km s}^{-1}, \sigma'_V = 10.5 \pm 3.3 \text{ km s}^{-1} \text{ kpc}^{-1}.
 \end{aligned}$$

In the above, the constants in the velocity and velocity-dispersion relations are evaluated at $z=2.2$ kpc, instead of $z=0$. This is the effective mean value of z for the sample over the fitting range from 1 to 4 kpc. Shifting the intercepts in this manner eliminates the correlation between the constant term and slope for these linear fits, simplifying the expression of the uncertainties in the two terms. For example, the linear description of $U(z)$ becomes $U = U|_{z=2.2} + U'(z-2.2)$, where z is in kpc, with similar expressions for V and for both components of the dispersion. Once again, we note that the choice of a linear description, in particular for the dispersion profiles, does not indicate that an intrinsically linear functional form is expected, merely that the data do not allow for the determination of higher-order terms. The linear descriptions given above are valid over the range $z = 1$ to 4 kpc.

The derived Thick-Disk scale height, velocity profiles, and velocity-dispersion profiles will be compared to results from other studies, and discussed further, in Section 5. First, though, we analyze our results in the context of a relatively simple model of the Galaxy, in

an effort to demonstrate that the derived intrinsic profiles are self-consistent, and possibly to constrain other fundamental Galactic parameters.

4. Equilibrium Model Comparison

Under the assumption of dynamical equilibrium, the Thick Disk velocity and velocity dispersion as functions of z are governed by the Galactic gravitational potential in which the Thick Disk resides. Are the measured velocity and dispersion profiles consistent with a condition of equilibrium and reasonable models for the Galactic potential? Can the profiles be used to constrain models of the Galaxy’s potential?

To address these questions, we derive expressions for the transverse velocity and velocity dispersion of a stellar Thick Disk in the presence of a parameterized model for the Galactic potential. The resulting relation between velocity and dispersion profiles is then used to investigate allowed values for the Galaxy-model parameters.

4.1. Formulation

In order to derive an expression for the rotational velocity, $v_\Theta(R, z)$, of a relaxed population of Thick Disk stars in equilibrium within the gravitational potential of the Galaxy, $\Phi_{tot}(R, z)$, we start with the Jeans equation:

$$\frac{1}{\rho_i} \frac{\partial(\rho_i \overline{v_R^2})}{\partial R} + \frac{1}{\rho_i} \frac{\partial(\rho_i \overline{v_R v_z})}{\partial z} + \frac{\overline{v_R^2} - \overline{v_\Theta^2}}{R} + \frac{\partial \Phi_{tot}}{\partial R} = 0 \quad (1)$$

Here R , Θ and z are galactocentric cylindrical coordinates, $\rho_i(R, z)$ is the volume density of a relaxed population of Thick Disk stars, and $\Phi_{tot}(R, z)$ is the total gravitational potential of the Galaxy. Defining velocity dispersions of the Thick Disk stars as

$$\begin{aligned} \overline{v_\Theta^2} &= \sigma_\Theta^2 + \overline{v_\Theta^2}, \\ \overline{v_R^2} &= \sigma_R^2 \end{aligned}$$

one can express the rotational velocity $\overline{v_\Theta}$ from Equation (1) as:

$$\overline{v_\Theta^2} = \sigma_R^2 \left(\frac{R}{\rho_i \sigma_R^2} \frac{\partial(\rho_i \sigma_R^2)}{\partial R} + \frac{R}{\rho_i \sigma_R^2} \frac{\partial(\rho_i \overline{v_R v_z})}{\partial z} + 1 - \frac{\sigma_\Theta^2}{\sigma_R^2} \right) + R \frac{\partial \Phi_{tot}}{\partial R} \quad (2)$$

Evaluation of the first term on the right side of Equation (2), the partial derivative with respect to R , requires knowledge of the R dependence of both the Thick-Disk number

density and the Thick-Disk velocity dispersion. We assume that the density distribution can be represented by exponential distributions in the radial and vertical directions,

$$\rho_i(R, z) = \rho_0 \exp(-(z/h_{z_{thick}} + R/h_{R_{thick}})),$$

where $h_{R_{thick}}$ and $h_{z_{thick}}$ are the respective scale length and scale height. Star counts from the APS Catalog (Larsen & Humphreys 2003) give an estimate for the radial scale length of the Thick-Disk number density of 4.7 ± 0.2 kpc. Analysis of SDSS data (Jurić et al 2005) gives a value of ~ 3.5 kpc. We shall explore values ranging from 3.5 to 5 kpc in our modeling.

There have been no attempts to estimate the radial scale length of the Thick-Disk velocity-dispersion profile. If the Thick Disk were self-gravitating, one would expect the square of the *vertical* velocity dispersion to be proportional to the density. If one further assumes that, as with the Thin Disk, the shape of the velocity ellipsoid of the Thick Disk is not varying with R at the solar circle, then $\sigma_R^2 \propto \sigma_z^2$. (For example, this is what one would expect if the scattering of individual Thick Disk stars is an isotropic process.) Consequently, this implies that σ_R^2 will also follow the Thick-Disk density distribution. Under these assumptions, the first term within the parentheses in Equation (2) would reduce to

$$-\frac{2R}{h_{R_{thick}}} \equiv -\Upsilon_a R. \quad (3a)$$

As will be discussed shortly, the total mass of the Thin Disk substantially exceeds that of the Thick Disk and, likewise, gradients in the potential in which the Thick Disk resides are expected to be dominated by the Thin-Disk mass distribution. Therefore, it may be more reasonable to assume that the vertical velocity dispersion of the Thick Disk stars will follow the mass distribution of the Thin Disk. Again, under the assumption of a non-varying shape of the Thick-Disk velocity ellipsoid, this implies the following form for the first term in Equation (2),

$$-\left(\frac{1}{h_{R_{thin}}} + \frac{1}{h_{R_{thick}}}\right)R \equiv -\Upsilon_b R, \quad (3b)$$

where $h_{R_{thin}}$ is the radial scale length of the Thin Disk.

These two alternative expressions for the factor Υ , Equations (3a) and (3b), are reasonable limiting cases for a generic thick disk. They represent the totally self-gravitating and the totally non-self-gravitating approximations, *i.e.* the latter assumes total dominance of an imbedded thin disk. The true nature of the Milky Way Thick Disk presumably lies somewhere between these limits. We will explore models that incorporate each of these two limiting cases.

The second term on the righthand side of Equation (2) is the z -gradient of the velocity dispersion cross-correlation, $\overline{v_R v_z}$. Binney and Tremaine (1987) discuss two extreme possibilities, when the velocity dispersion ellipsoid’s principal axes remain aligned with the radial coordinate of the galactocentric cylindrical system, R , and when the ellipsoid’s principal axes remain aligned with the radial direction of the spherical system of coordinates. In the first case, $\overline{v_R v_z}$ is independent of z , and in the second case, the cross-term can be approximated as

$$\overline{v_R v_z} \approx 0.5 \sigma_R^2 \frac{z}{R_\odot}.$$

Taking into account that the vertical scale height of the Thick Disk is smaller than its radial scale length, the cross-term in Equation (2) can be approximated as:

$$\frac{R}{\rho_i \sigma_R^2} \frac{\partial(\rho_i \overline{v_R v_z})}{\partial z} \approx 0.5 \left(1 - \frac{z}{h_{z_{thick}}} \right)$$

The contribution to the disk rotation by the velocity dispersion cross-term is small but non-negligible. We shall model the equilibrium of the Thick Disk rotation with, and without the cross-term.

The remaining term within the parentheses in Equation (2), $\sigma_\theta^2 / \sigma_R^2$, is known from the proper-motion/photometry analysis for our Thick Disk sample. This leaves only the gravitational potential to be evaluated.

The gravitational potential, Φ_{tot} , is the sum of the Disk potential and the potential of the Halo, $\Phi_{tot}(R, z) = \Phi_{disk}(R, z) + \Phi_{halo}(R, z)$. The Disk potential is in turn a combination of the Thin-Disk gravitational potential and a contribution from the Thick Disk. The Disk potential reflects the total mass of each disk component, which is roughly proportional to the product of its density in the plane with its vertical scale height. Estimates of the density of the Galactic Thick Disk are rather uncertain, with values of the thick-to-thin local density ratio varying from about two percent (Gilmore 1984) to about twenty percent (Fuhrmann 2004) with most of the recent estimates being in the range 3.5 to 7 percent (Robin et al. 1996, Ojha et al. 2001, Du et al. 2003). On the other hand, with an “exponential” scale height of ~ 280 kpc (Korchagin et al. 2003), the vertical scale of the Thin Disk is perhaps one third to one quarter that of the Thick Disk. Thus, the total mass of the Thin Disk is significantly greater than that of the Thick Disk. Summarizing existing starcount studies, Siegel et al. (2002) find most of these indicate the Thick Disk comprises roughly 10% of the mass of the Thin Disk. Furthermore, with the Thick Disk’s presumed larger radial scale length, its contribution to the gradient of the total Galactic potential will be even less still. For these reasons, we choose to neglect the Thick Disk’s contribution to the gravitational potential in studying its equilibrium. As such, we need only specify models for the Thin Disk potential and the Halo potential.

Making this explicit, and adopting expressions for the other terms as discussed above, Equation (2) becomes

$$\overline{v_{\Theta}^2}(z) = \sigma_R^2(z) \left[-\Upsilon_{a,b}R + 0.5\lambda \left(1 - \frac{z}{h_{z_{thick}}} \right) + 1 - \frac{\sigma_{\Theta}^2}{\sigma_R^2} \right] + R \frac{\partial \Phi_{halo}}{\partial R} + R \frac{\partial \Phi_{disk}}{\partial R} \quad (4)$$

where $\Upsilon_{a,b}$ assumes the form of either Equation (3a) or (3b) and λ is set to 1 or 0 depending on whether or not one chooses to include the velocity-dispersion cross-term. It now remains to adopt reasonable models for the Thin Disk and Halo potentials.

4.1.1. Thin Disk potential

Assuming the surface-density distribution of the Thin Disk to be exponential, $\Sigma_{thin}(R) = \Sigma_0 \exp(-R/h_{R_{thin}})$, we can express its gravitational potential in terms of the Bessel function (Toomre 1962),

$$\Phi_{disk}(R, z) = -2\pi G \Sigma_0 h_{R_{thin}}^2 \int_0^{\infty} \frac{J_0(kr) \exp(-k|z|) k dk}{[1 + k^2 h_{R_{thin}}^2]^{3/2}}. \quad (5)$$

We define that portion of the Thick Disk rotation associated with the Thin-Disk gravitational potential to be v_{disk}^2 , which can be expressed with the help of Equation (5) as

$$v_{disk}^2(R, z) \equiv R \frac{\partial \Phi_{disk}}{\partial R} = 2\pi G \Sigma_0 h_{R_{thin}}^2 R_{\odot} \int_0^{\infty} \frac{J_1(kR) \exp(-k|z|) k dk}{[1 + k^2 h_{R_{thin}}^2]^{3/2}}. \quad (6)$$

In the mid-plane of the disk, the integral in Equation (6) can be evaluated, and written in terms of the modified Bessel functions I_i, K_i (Freeman 1970):

$$v_{disk}^2(R_{\odot}, 0) = 4\pi G \Sigma_0 h_{R_{thin}} x^2 \left[I_0(x) K_0(x) - I_1(x) K_1(x) \right], \quad (7)$$

where $x = R_{\odot}/2h_{R_{thin}}$.

4.1.2. Halo potential

We consider the two simplest halo potential models, the Plummer model (see Binney & Tremaine 1987) and the pseudo-isothermal model (see Bahcall & Soneira 1980). The Plummer model potential is given by the expression

$$\Phi_{halo} = -\frac{GM_H}{(r^2 + a^2)^{1/2}}, \quad (8)$$

where r is Galactocentric distance, G is the gravitational constant, M_H is the total mass of the halo, and a is the core radius. The total halo mass can be expressed in terms of the rotational velocity of the local standard of rest, v_c , which is determined by the combined disk and halo gravitational potentials in the solar neighborhood,

$$v_c^2 = \frac{GM_H R_\odot}{(R_\odot^2 + a^2)^{3/2}} + v_{disk}^2(R_\odot, 0). \quad (9)$$

Solving for the mass of the halo, M_H , in Equation (9) and substituting it into Equation (4) yields

$$\begin{aligned} \overline{v_\Theta}^2(z) = \sigma_R^2(z) & \left[-\Upsilon_{a,b}R + 0.5\lambda \left(1 - \frac{z}{h_{zthick}} \right) + 1 - \frac{\sigma_\Theta^2}{\sigma_R^2} \right] \\ & + \frac{(v_c^2 - v_{disk}^2(R_\odot, 0))(R_\odot^2 + a^2)^{3/2}}{(R_\odot^2 + z^2 + a^2)^{3/2}} + v_{disk}^2(R_\odot, z), \end{aligned} \quad (10)$$

where the portion of the rotational velocity associated with the disk potential, both in and out of the plane, $v_{disk}^2(R_\odot, 0)$ and $v_{disk}^2(R_\odot, z)$, are given by Equations (6) and (7).

If, instead, a pseudo-isothermal model of the halo potential is assumed (Bahcall & Soneira 1980), expressions for the Thick-Disk rotational velocity can be derived in a similar manner. For this model, the halo potential is given by the expression

$$\Phi_{halo} = 4\pi G \rho_0 a^2 \left[1 - \frac{a}{r} \operatorname{atan} \frac{r}{a} \right], \quad (11)$$

where ρ_0 is the central density of the halo. The Thick-Disk rotational velocity then becomes

$$\begin{aligned} \overline{v_\Theta}^2(z) = \sigma_R^2(z) & \left[-\Upsilon_{a,b}R + 0.5\lambda \left(1 - \frac{z}{h_{zthick}} \right) + 1 - \frac{\sigma_\Theta^2}{\sigma_R^2} \right] + \\ & \left(\frac{v_c^2 - v_{disk}^2(R_\odot, 0)}{(a/R_\odot) \operatorname{atan}(R_\odot/a) - (1 + R_\odot^2/a^2)^{-1}} \right) \left[\frac{a}{(R_\odot^2 + z^2)^{1/2}} \operatorname{atan} \frac{(R_\odot^2 + z^2)^{1/2}}{a} - \frac{1}{1 + (R_\odot^2 + z^2)/a^2} \right] \\ & + v_{disk}^2(R_\odot, z), \end{aligned} \quad (12)$$

where $v_{disk}^2(R_\odot, 0)$ and $v_{disk}^2(R_\odot, z)$ are given by Equations (6) and (7).

4.2. Results

Equations (10) or (12), depending on one's choice of Halo potential, express the equilibrium relationship between the Thick-Disk rotational velocity, $\overline{v_\Theta}(z)$, and the radial component of its velocity dispersion, $\sigma_R(z)$. We wish to test whether or not the intrinsic Thick Disk velocity and dispersion profiles derived from our sample are consistent with these relations.

The profiles to be tested are those given in Section 3.4 by the parameters ($V|_{z=2.2}$, V' , $\sigma_U|_{z=2.2}$, and σ'_U), which are valid descriptions over the range $1 < Z < 4$ kpc. As the relative uncertainties of the $V \equiv \overline{v_\Theta}$ profile are smaller than those of $\sigma_U \equiv \sigma_R$, we elect to adopt the former, insert into Equations (10) and (12), and then solve for the resultant dispersion profile. The “model” dispersion profile can then be compared to that derived from our measures, over the appropriate range in z .

In order to do so, various parameters of our equilibrium model must be specified. Values for these are taken from the literature as follows.

The Thin Disk contribution to the Galactic potential can be calculated given its radial scale length, $h_{R_{thin}}$, and its mass surface density in the solar neighborhood, $\Sigma_{thin}(R_{sun})$. The Thin-Disk radial scale length is better determined than that of the Thick Disk. Recent estimates, (see e.g., Jurić et al. 2005), give a value of 2.4 ± 0.2 kpc. We adopt $h_{R_{thin}} = 2.5$ kpc. Korchagin et al. (2003) estimate the surface density of the Thin Disk in the solar neighborhood to be $42 \pm 6 M_\odot \text{ pc}^{-2}$. We shall explore values ranging from 36 to $48 M_\odot \text{ pc}^{-2}$. The value of R_{sun} is taken to be 8 kpc.

The Thick-Disk radial scale length, $h_{R_{thick}}$, is one of the key parameters that determines the rotational equilibrium of the Thick Disk stars. Estimates, based on star counts, range from 2.5 ± 0.3 kpc (Robin et al. 1996) to 4.3 ± 0.7 kpc (Larsen & Humphreys 2003). A recent determination based on the Sloan Digital Sky Survey data gives a value of 3.5 ± 1 kpc (Jurić et al. 2005). We will allow the value of $h_{R_{thick}}$ to vary from 3.5 to 5.0 kpc.

As mentioned in Section 4.1, we shall explore two different expressions for the Thick-Disk pressure term, Equations (3a) and (3b). These represent the limiting cases of behavior of the Thick Disk in terms of the radial scale length of its velocity dispersion, i.e., does it more resemble a self-gravitating disk, (3a), or a disk responding to the external potential of the Thin Disk, (3b).

Another uncertainty is the inclusion of the velocity-dispersion cross-term, regulated in Equations (10) and (12) by the factor λ . We will generate models both with and without the cross-term included. When included, the value for the Thick Disk’s vertical scale height is set to 0.785 kpc, as derived in Section 3.4.

Another of the terms that appears in Equations (10) and (12) is the Thick-Disk velocity-dispersion ratio, σ_Θ/σ_R . Other studies find this ratio to be on the order of one, or slightly less than one, in the solar neighborhood. (See for instance Beers & Sommer-Larsen (1995) and Chiba & Beers (2000).) As can be seen from Figure 6, our measures agree and indicate that the ratio does not vary drastically as a function of z . We will adopt our measures for this ratio, as given by the derived intrinsic dispersion profiles of Section 3.4.

The final model parameters to be specified are those related to the Halo. A spherically symmetric halo is typically determined by two parameters - the central density of the halo and its core radius. Donato et al. (2004) studied the mass distribution in a sample of 25 disk galaxies of different morphological types using high-resolution rotation curves. They find a strong correlation between the halo core radius, a , and the thin-disk exponential scale length, $h_{R_{thin}}$, namely $a[\text{kpc}] \approx 13(h_{R_{thin}}[\text{kpc}]/5)^{1.05}$. Using this relation, the Halo core radius of the Milky Way is about 6.3 kpc. We assume this value in our models. The central density of the dark matter Halo can be expressed via the rotational velocity of the local standard of rest, v_c , taking into account a contribution from the Thin-Disk gravitational potential given by Equation (9). In our models, 220 km s^{-1} is assumed for the velocity of the local standard of rest. And, of course, the choice of Equation (10) or Equation (12) reflects a choice of the form of the Halo potential, i.e., that of a Plummer model or that of a pseudo-isothermal model. Both will be examined.

Table 1 indicates the parameters used to calculate 32 equilibrium models of the Thick Disk based on Equations (10) and (12) and our measured V -velocity profile from Section 3.4. Each model generates a U -dispersion profile that is consistent with the input V -velocity profile under the condition of equilibrium. These calculated U -dispersion profiles are plotted in Figure 8, and labeled by model number, as given in Table 1.

Within each panel of Figure 8 are four model profiles, corresponding to the upper and lower limits considered for the values of the Thick-Disk scale length and the Thin-Disk surface density. Red curves are models with $h_{R_{thick}}=3.5 \text{ kpc}$, while blue curves are with $h_{R_{thick}}=5.0 \text{ kpc}$. Dashed curves are models with $\Sigma_{thin}(R_{sun})=36 \text{ M}_{\odot}/\text{pc}^2$, while solid curves have $\Sigma_{thin}(R_{sun})=48 \text{ M}_{\odot}/\text{pc}^2$. The column of four panels on the left represents a Plummer Halo potential while the rightside column assumes a pseudo-isothermal form. Models in the top four panels employ the “self-gravitating” form for the pressure term, i.e., Equation (3a), while the bottom four panels are of models using the “external” form, Equation (3b). Finally, panels in the first and third rows are of models with no velocity-dispersion cross-term, while those in the second and fourth rows include the cross-term. Also shown in each panel, for the sake of comparison, is the 1-sigma error range for the intrinsic U -dispersion profile derived from the observed SGP proper-motion sample.

General trends seen in Figure 8 are worth noting. The form of the pressure term, either Equation (3a) or (3b), affects the σ_U dispersion profile significantly. The lower four panels, which are based on the assumption that the Thick Disk sits within an “external” (Thin Disk) potential, reveal consistently lower dispersion profiles. Also, these models tend to be insensitive to the other Galactic parameters such as the value of the local surface density, the radial scale length of the Thick Disk, or the functional form of the Halo potential. Conversely,

Table 1. Equilibrium model parameters

1	2	3	4	5	6	1	2	3	4	5	6
Run #	$h_{R_{thick}}$ (kpc)	Σ_{thin} (M_{\odot}/pc^2)	Pl/iso	λ	a/b	Run #	$h_{R_{thick}}$ (kpc)	Σ_{thin} (M_{\odot}/pc^2)	Pl/iso	λ	a/b
01	3.5	36.0	Pl	0	a	05	3.5	36.0	iso	0	a
02	5.0	36.0	Pl	0	a	06	5.0	36.0	iso	0	a
03	3.5	48.0	Pl	0	a	07	3.5	48.0	iso	0	a
04	5.0	48.0	Pl	0	a	08	5.0	48.0	iso	0	a
09	3.5	36.0	Pl	1	a	13	3.5	36.0	iso	1	a
10	5.0	36.0	Pl	1	a	14	5.0	36.0	iso	1	a
11	3.5	48.0	Pl	1	a	15	3.5	48.0	iso	1	a
12	5.0	48.0	Pl	1	a	16	5.0	48.0	iso	1	a
17	3.5	36.0	Pl	0	b	21	3.5	36.0	iso	0	b
18	5.0	36.0	Pl	0	b	22	5.0	36.0	iso	0	b
19	3.5	48.0	Pl	0	b	23	3.5	48.0	iso	0	b
20	5.0	48.0	Pl	0	b	24	5.0	48.0	iso	0	b
25	3.5	36.0	Pl	1	b	29	3.5	36.0	iso	1	b
26	5.0	36.0	Pl	1	b	30	5.0	36.0	iso	1	b
27	3.5	48.0	Pl	1	b	31	3.5	48.0	iso	1	b
28	5.0	48.0	Pl	1	b	32	5.0	48.0	iso	1	b

¹Model run number

²Thick-Disk radial scale length

³ocal Thin-Disk mass surface density

⁴Halo potential functional form; Plummer or isothermal

⁵Velocity-dispersion cross-term factor

⁶Form of the pressure term; Equation (3a) or (3b)

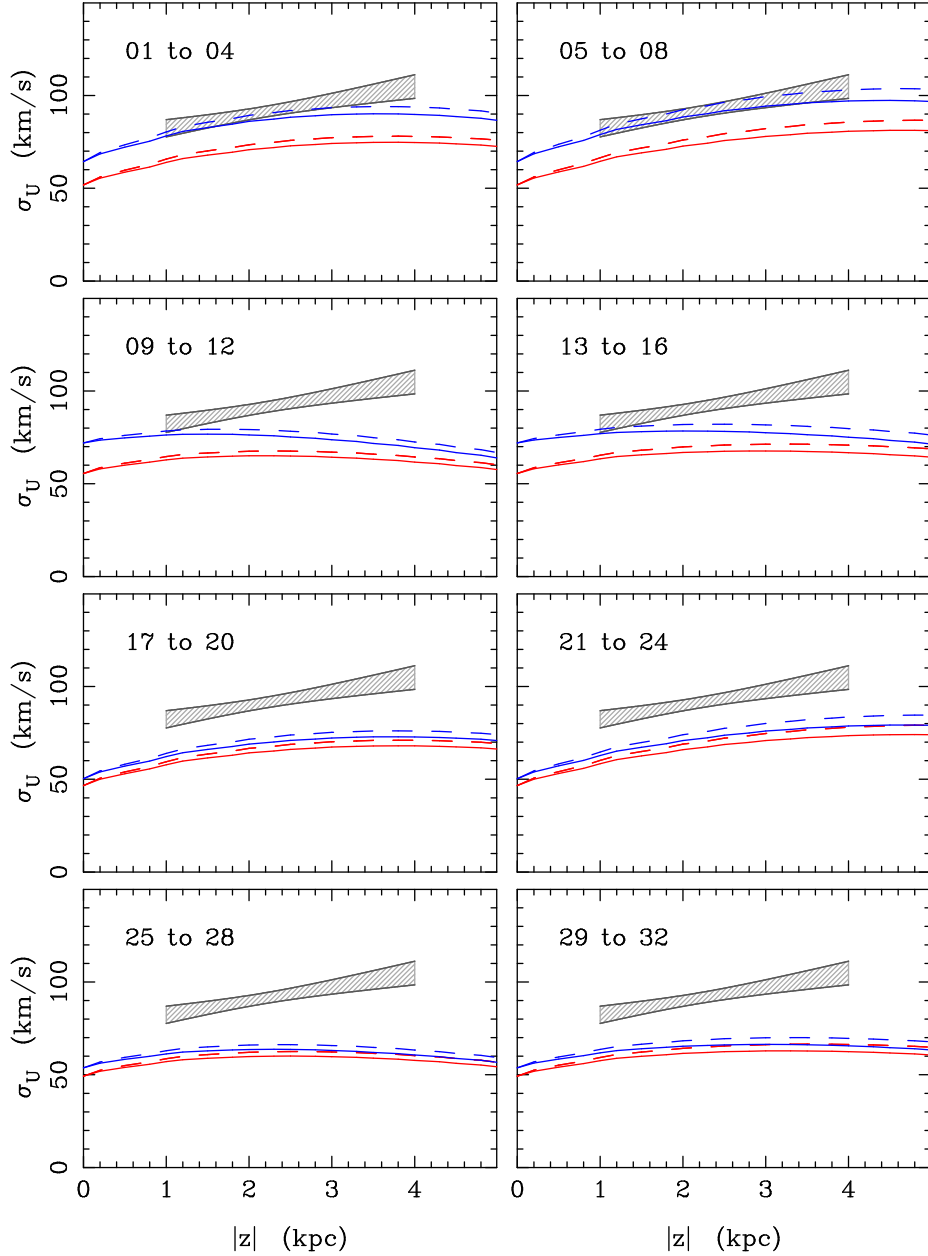


Fig. 8.— Velocity dispersion, σ_U , as a function of z , assuming our equilibrium model and the V -velocity profile derived for our sample. The 32 models shown correspond to those listed in Table 1 and explore limiting values of five uncertain parameters of the equilibrium model. Within each panel, the blue(/red) curves correspond to a value of the Thick-Disk radial scale length of 5.0(/3.5) kpc. The solid(/dashed) curves are of models with the local surface density set to 48(/36) M_\odot/pc^2 . The values of the remaining parameters can be inferred from the corresponding model numbers in Table 1. Also, within each panel is shown the ± 1 -sigma error range in the intrinsic U -dispersion derived for our SGP sample.

in the top four panels, in which the pressure term is that to be expected for a self-gravitating disk, the curves are sensitive to the assumed value for the Thick-Disk radial scale length, and, to a lesser extent, the form of the Halo potential.

In all cases, models that include the velocity-dispersion cross-term, $\overline{v_R v_z}$, yield profiles that are relatively depressed, either remaining level or decreasing slightly from $z = 1$ to 4 kpc. This is in contrast to the behavior of the derived intrinsic dispersion profile based on our sample.

Judging from Figure 8, the Thick Disk velocity and velocity-dispersion profiles derived from our SGP sample are consistent with one another and with the condition of equilibrium for at least some subset of reasonable values of the various Galactic structure parameters. In particular, the upper pair of curves in each of the two top panels fit the data reasonably well. These curves represent models with no velocity-dispersion cross-term, with the “self-gravitating” form of the pressure term, and with the higher estimate for the Thick-Disk radial scale length. The pseudo-isothermal Halo model, the right panel, provides a better fit to the data, although the Plummer-model fit is also acceptable. The fits are largely insensitive to the value of the local surface density of the Thin Disk, i.e., dashed versus solid curves.

We note that it is somewhat unsettling that the best fitting models are those that assume the “self-gravitating” form of the pressure term for the Thick Disk. Certainly a disk that has embedded within it another disk that is substantially more massive would not be expected to be self-gravitating, and we think it unlikely that the Galactic Thick Disk is self-gravitating. The underlying property of the models employing Equation (3a) is that their pressure radial scale length is substantially larger than the mass scale length of the Thin Disk, approximately by a factor of two. Rather than assuming a direct link to the radial scale length of the Thick Disk’s mass distribution and self-gravitation, this might also represent a failure of a second assumption inherent in Equation (3a), that the shape of the Thick-Disk velocity ellipsoid remains unchanging as a function of R in the local neighborhood. This, in turn, might be due to scattering of Thick Disk stars that is non-isotropic, perhaps by dense spiral arms. This is purely speculative, though. Further proper-motion studies at low Galactic latitudes, combined with radial-velocity measures, would help address the nature of the Thick Disk’s velocity ellipsoid and its spatial variation.

5. Discussion

5.1. Comparison to Previous Studies

Our estimate of the Thick-Disk scale height, 783 ± 48 pc, is consistent with previous determinations from other star-count studies, albeit possibly on the low end of said range. Buser et al. (1999), in their Table 5, and Siegel et al. (2002), in their Table 1, provide summaries of previous estimates of the Thick-Disk scale height. Values range from 700 to 2000 pc, with most estimates falling between 800 and 1200 pc. More recently, a study by Cabrera-Lavers et al. (2005), identifying Red Clump stars from 2MASS data, yields a value of 1062 ± 52 pc. Using SDSS data, Jurić et al. (2005) find a value of 1200 pc, based on dwarf stars within 1.5 kpc of the Sun. Siegel et al. (2002) point out the inverse correlation between derived scale height and local density normalization in some Thick-Disk modeling studies. Because of the manner in which our SGP sample was selected, we do not attempt to estimate the local density of the Thick Disk component.

The rotational lag of the Thick Disk has been measured in a number of studies. Majewski (1993) summarizes those made prior to 1993 in his Figure 7 of that review. These estimates vary substantially, from roughly -20 km s⁻¹ to -120 km s⁻¹, and with a suggestion of a correlation with z , the larger lag values being found for samples at larger z . Several of the studies that Majewski references fall nicely along our relation of z and Thick Disk lag. Among these are the studies of Norris (1986), Wyse & Gilmore (1990), and Beers et al. (1992). Several other studies, specifically those of Murray (1986) and of Hanson (1989) obtain values for the z gradient in lag that are similar to what we find. While not all of these z -gradient studies isolate the Thick Disk stars in their samples, as Majewski (1993) argues, it is unlikely that Halo contamination can account entirely for the observed gradient. In Majewski’s (1992) proper-motion study of the North Galactic Pole (NGP), the Thick Disk is fit through multi-component modeling. He finds a somewhat lower gradient in the lag, -21 ± 1 km s⁻¹ kpc⁻¹. More recently, in a full space-motion study by Chiba & Beers (2000), in which the Thick Disk component is separated by metallicity, they obtain the same value for the gradient as do we, -30 ± 3 km s⁻¹ kpc⁻¹. In another 3-d velocity study, at the NGP, Soubiran et al. (2003) do detect a separate Thick Disk component, via the kinematics, but do not see overwhelming evidence for a z gradient, although this is not ruled out. Instead they present a single value of -51 ± 5 km s⁻¹ as representative of their Thick Disk sample. Gilmore et al. (2002) analyze radial velocities at intermediate-latitude lines-of-sight along Galactic rotation and anti-rotation. Their model of the velocity distribution fits the observations much better when their fainter, more distant sample is modeled using a Thick Disk with a substantial rotational lag, i.e., -100 km s⁻¹. Wyse et al. (2006), further examine the samples along these lines-of-sight and again see evidence of a high-lag component, ~ -120 km s⁻¹, in

addition to a “canonical” Thick Disk with a constant lag of -40 km s^{-1} . We note, however, that the excess they observe might very well be explained by a Thick Disk component with substantial lag and z -gradient, such as our SGP sample implies.

It does not seem likely that Halo contamination can account for the large z -gradient that we observe in the lag. Our sample’s number-density profile provides an estimate of the Halo contamination, a modest $8 \pm 6 \%$, and this has been included in our simulated samples from which the intrinsic Thick Disk lag was derived. Nor is it likely that random errors in the proper motions or in the distance estimates would lead us to overestimate the lag and its gradient. These uncertainties have very little effect on the observed V profile, because of the geometry involved and the simple relationship between distance, proper motion, and velocity. A systematic error in the absolute proper-motions would translate directly into a systematic error in the V -velocity gradient. The estimated uncertainty in the proper-motion system of the SPM3 is 0.4 mas yr^{-1} , corresponding to an error of only $2 \text{ km s}^{-1} \text{ kpc}^{-1}$ in the z -gradient of either of the tangential-velocity profiles.

Such a systematic error could account for the marginally significant gradient found in the U velocity, $4.8 \pm 2.9 \text{ km s}^{-1} \text{ kpc}^{-1}$. A flat U -velocity profile is consistent with disklike motion for the sample. The offset of $19.1 \pm 2.7 \text{ km s}^{-1}$ is presumably a reflex of the peculiar motion of the sun in this direction. Although, this value is larger than expected when compared to the Hipparcos-based value of 10.0 ± 0.4 determined by Dehnen & Binney (1998).

While the velocity profiles are sensitive to systematic errors, it is the random errors in both proper motion and distance estimates that affect the observed velocity-dispersion profiles. Figure 9 shows the resultant “observed” U -dispersion profile of our best-fit model, in comparison to the underlying intrinsic profile. The profile is significantly steepened, illustrating the need for accurate knowledge of the observational uncertainties when attempting to discern the intrinsic velocity dispersion.

With this in mind, the velocity dispersions we derive show a modest z -gradient of about $+9 \text{ km s}^{-1} \text{ kpc}^{-1}$ over the range $1 < z < 4$. At our sample’s mean distance of $z=2.2 \text{ kpc}$, the dispersions are roughly 90 and 70 km s^{-1} in σ_U and σ_V , respectively. This can be compared to the velocity dispersion of the intermediate-metallicity sample of Chiba & Beers (2000), which they identify with the Thick Disk. They find σ_V increases from roughly 40 km s^{-1} near the plane, to a value of about 70 km s^{-1} at $z = 0.5 \text{ kpc}$, remaining constant after that out to their sample’s limiting distance of $z = 1.75 \text{ kpc}$. Majewski (1994) has summarized the results of six different proper-motion studies toward the Galactic Poles. He shows in his Figure 1 the z dependence of σ_U and σ_V from these studies. It is important to note that these samples include *all* stars, with no attempt to isolate Thick Disk members, although over some range of z the Thick Disk should dominate naturally. The various studies agree reasonably well,

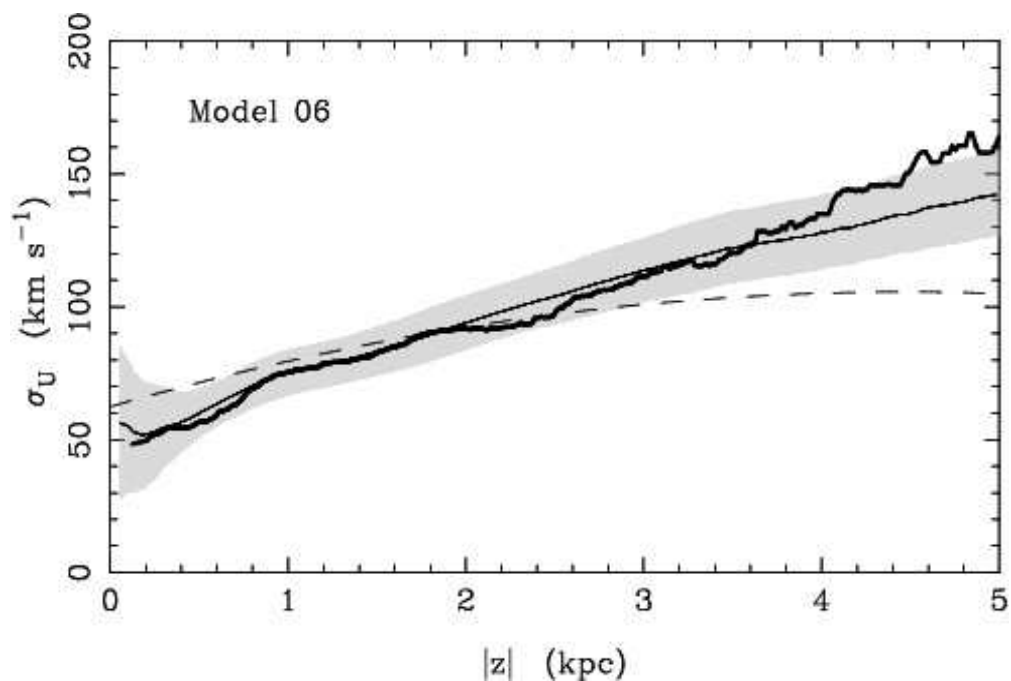


Fig. 9.— Intrinsic and “observed” velocity dispersions, σ_U , as a function of z , for the best-fit equilibrium model, #06. The dashed curve shows the intrinsic dispersion profile that results from this model. The thin solid curve, with ± 1 -sigma error bars shown in gray, indicates the mean of 100 Monte-Carlo simulated datasets based on this intrinsic dispersion profile. The heavier, irregular line shows the σ_U profile observed for the actual SGP red-giant sample.

showing a linear increase in σ_U and σ_V from 10 to 20 km s⁻¹ in the solar neighborhood to approximately 70 to 100 km s⁻¹ at $z = 2$ kpc. This steep gradient is presumably due to the Thin Disk stars' lower velocity dispersion in the solar neighborhood. On the other hand, the general agreement with our derived dispersions near $z = 2$ kpc suggests that the Thick Disk dominates all samples at this range. In Majewski's (1992) study, where an effort *is* made to isolate the Thick Disk stars, a gradient of ~ 12 km s⁻¹ kpc⁻¹ is found out to $z = 4$ kpc, similar to what we obtain.

5.2. Implied Nature of the Thick Disk

The original notion of thick disks was introduced in the surface-photometry studies of S0 galaxies by Burstein (1979) and Tsikoudi (1979). Subsequent observations, both Galactic and extragalactic, have begun to provide an understanding of the nature and possible formation processes of thick disks. The current picture for disk galaxies is detailed in Yoachim & Dalcanton (2006) and references therein. In short, they find that thick disks are a somewhat regular component of disk galaxies, that the scale heights and scale lengths of thick disks exceed those of their embedded thin disks by factors of 1.25 and 2, respectively, and that they are made up of old, metal-poor stars, (see also Mould et al. 2005, Davidge 2005, Tikhonov et al. 2005). Yoachim & Dalcanton also find that, for less massive galaxies, the thick disk contributes significantly (up to half) to the luminous mass. From the kinematical analysis of two different disk galaxies, Yoachim & Dalcanton (2005) find that the thick disk rotates at 30 – 40% of the rotation speed of the thin disk in one of the galaxies, while in the second, the thick disk seems to counterrotate, if it rotates at all.

With regard to the Thick Disk of our own Galaxy, there is mounting evidence that the Thick Disk's chemical abundance profile is distinct from that of the Thin Disk, (for a more thorough discussion, see Brewer & Carney 2006 and references therein). Specifically, Thick Disk stars have a ratio $[\alpha/\text{Fe}]$ for given Fe that is systematically higher than the $[\alpha/\text{Fe}]$ ratio for Thin Disk stars. Also, there is little or no gradient in metallicity as a function of distance from the Galactic plane, (Gilmore et al. 1995, Rong et al. 2001). These properties point to the Thick Disk being a system that is distinct from the present Thin Disk.

There are a large number of studies that have attempted to model the formation of the Galactic Thick Disk. Briefly, these can be classified into three main groups: 1) the Thick Disk is the precursor of the Thin Disk, and was formed from gas at a large scale height that settled in a slow, pressure-supported collapse (see e.g., Gilmore & Wyse 1986, Burkert et al. 1992), 2) the Thick Disk formed from a pre-existing Thin Disk by a heating mechanism, the most viable of which is energy deposited by the accretion of a dense satellite (see e.g.,

Quinn et al. 1993, Velazquez & White 1999), although other mechanisms have been proposed (Kroupa 2002), and 3) the Thick Disk is formed from the accretion and disintegration of satellites during an early and active period of hierarchical clustering (Abadi et al. 2003, Brook et al. 2004). This last scenario relies on satellites having orbits highly coupled with the disk rotation, i.e., orbits of high circularity and/or that are strongly circularized due to dynamical friction.

The evidence from chemical abundances of Thick Disk stars appears to favor either of the last two scenarios. Further distinguishing between these last two types of formation might be possible by comparing the observed kinematical profiles of the Thick Disk to formation models. Among recent simulations, there are regrettably few that present velocity-lag and velocity-dispersion profiles. Instead, these works tend to emphasize the density profile, chemical abundance pattern and vertical velocity dispersion as a function of age, and generally present simple means for the tangential velocity dispersions. A meaningful comparison of our results to theoretical models is therefore difficult. However, we mention two examples that might serve as starting points for more comprehensive kinematical comparisons between formation models and observations.

The study of Abadi et al. (2003) does present a prediction for the rotational lag of the combined disks as a function of z . Interestingly, their Figure 5 indicates a gradient of ~ -20 km s⁻¹ kpc⁻¹ in the range $2 < z < 4$ kpc where the thick disk dominates. In the Abadi et al. simulations, well over half of the thick-disk stars are the debris from disrupted satellites, circularized through dynamical friction before being absorbed.

The second example we note is that of Velazquez & White (1999). This study analyzes the thickening of a pre-existing thin disk due to the accretion of a single, dense, massive (20% of the mass of the disk) satellite. While not presenting the resulting “thick-disk” velocities or velocity dispersions as a function of z , they do show the R profiles of the velocity dispersions. In particular, from their Figure 5, the R -gradient of σ_U for the resulting thick disk is slightly shallower than that of the precursor thin disk. We note that qualitatively this is in agreement with our equilibrium modeling, for which the best fits were found using the form of the pressure term that corresponds to a shallower gradient, our Equation (3a).

Although we are unable to distinguish between current scenarios for Thick Disk formation at this time, we urge those who construct such models to present the resulting z profiles of the various velocity components and dispersions. The observational constraints provided by proper-motion studies such as this one, as well as radial-velocity studies, will only continue to improve with time.

6. Summary

SPM3 absolute proper motions are combined with 2MASS near-infrared photometry for a photometrically-selected sample of ~ 1200 stars at the South Galactic Pole. It is shown that these stars are predominantly Thick-Disk red giants. Photometric distances and tangential velocity distributions are determined for the sample using a Monte-Carlo modeling method that automatically corrects for bias due to distance errors. From this modeling, the intrinsic properties of the Thick Disk are derived as a function of distance from the Galactic plane over the range $1 < z < 4$ kpc.

The vertical scale height of the Thick Disk is found to be 783 ± 48 pc. The rotational lag shows a linear variation with z , having a gradient of -30.3 ± 3.2 km s $^{-1}$ kpc $^{-1}$ and a value of -91.6 ± 1.9 km s $^{-1}$ at the samples' mean distance of 2.2 kpc. The tangential velocity dispersions also show a variation with z , although with a much shallower slope of about 9 ± 3 km s $^{-1}$. Under the assumption of dynamical equilibrium, the V -velocity profile and (primarily) U -velocity dispersion profile as functions of z are constrained by the Galactic potential within which the Thick Disk resides. We have shown that for reasonable parameters of the dominant Galactic components, i.e., the Halo and Thin Disk, the kinematics of the Thick Disk as derived from our observed sample are self-consistent. Our modeling also indicates preference for a Thick-Disk velocity ellipsoid with zero cross term, i.e., one whose axes remain parallel to the Galactic plane independent of z . The tangential velocity and velocity-dispersion profiles presented here should be able to better constrain theoretical models of Thick Disk formation.

We are grateful to an anonymous referee for making a number of helpful comments, among them, the suggestion to include the reduced proper motion diagram. van Altena wishes to thank Dr. M. Miyamoto and Dr. M. Yoshizawa for the opportunity to spend a sabbatical semester, back in 1995, at the National Astronomical Observatory in Mitaka, Japan. Discussions with them and co-author Korchagin were important to initiating this research. This publication makes use of data products from the Two Micron All Sky Survey. The Yale/San Juan SPM program has been supported over the years by a number of grants from the National Science Foundation, the most recent of these being NSF grants 0098548 and 0407293.

REFERENCES

- Abadi, M. G., Navarro, J. F., Steinmetz, M., & Eke, V. R. 2003, *ApJ*, 597, 21
Allende Prieto, C., Beers, T. C., Wilhelm, R., Newberg, H. J., Rockosi, C. M., Yanny, B.,

- Lee, Y. S. 2006, *ApJ*, 636, 804
- Bahcall, J. N., & Soneira, R. M. 1980, *ApJS*, 44, 73
- Beers, T. C., Doinidis, S. P., Griffin, K. E., Preston, G. W., Sackett, S. A. 1992, *AJ*, 103, 267
- Beers, T. C. & Sommer-Larsen, J. 1995, *ApJS*, 96, 175
- Binney, J., & Tremaine, S. 1987, *Galactic Dynamics*, (Princeton: Princeton Univ. Press)
- Bland-Hawthorn, J., & Freeman, K. 2004, *PASA*, 21, 110
- Brewer, M. M., & Carney, B. W. 2004, *PASA*, 21, 134
- Brewer, M. M., & Carney, B. W. 2006, *AJ*, 131, 431
- Brook, C. B., Kawata, D., Gibson, B. K., & Freeman, K. C. 2004, *ApJ*, 612, 894
- Burkert, A., Truran, J. W., & Hensler, G. 1992, *ApJ*, 391, 651
- Burstein, D. 1979, *ApJ*, 234, 829
- Buser, R., Rong, J., & Karaali, S. 1999, *A&A*, 348, 98
- Cabrera-Lavers, A., Garzón, F., & Hammersley, P. L. 2005, *A&A*, 433, 173
- Carney, B. W., Latham, D. W., & Laird, J. B. 1989, *AJ*, 97, 423
- Chen, B., Stoughton, C., Smith, J. A., et al. 2001, *ApJ*, 553, 184
- Chiba, M., & Beers, T. C. 2000, *AJ*, 119, 2843
- Dehnen, W. & Binney, J. J. 1998, *MNRAS*, 298, 387
- Donato, F., Gentile, G., & Salucci, P. 2004, *MNRAS*, 353, L17
- Du, C., Zhou, Hu, Ma, Jun, et al. 2003, *A&A*, 407, 541
- Eggen, O. J., Lynden-Bell, D., & Sandage, A.R. 1962, *ApJ*, 136, 748
- Freeman, K. C. 1970, *ApJ*, 160, 811
- Fuhrmann, K. 1998, *A&A*, 338, 161
- Fuhrmann, K. 2004, *Astron.Nachr.*, 325, 3
- Gilmore, G., & Wyse, R. F. G., & Norris, J. E. 2002, *ApJ*, 574, L39
- Gilmore, G. 1984, *MNRAS*, 207, 223
- Gilmore, G., & Wyse, R. F. G. 1986, *Nature*, 322, 806
- Gilmore, G., Wyse, R. F. G., & Jones, J. B. 1995, *AJ*, 109, 1095
- Gilmore, G., & Reid, N. 1983, *MNRAS*, 202, 1025

- Girard, T. M., Dinescu, D. I., van Altena, W. F., Platais, I., Monet, D. G., & López, C. E. 2004, *AJ* 127, 3060
- Hamaker, H. C. 1978, *Applied Statistics*, 27, 76
- Hanson, R. B. 1989, *BAAS*, 21, 1107
- Holmberg, J., & Flynn, C. 2000, *MNRAS*, 313, 209
- Jackson, T., Ivezić, Z., & Knapp, G. R. 2002, *MNRAS*, 337, 749
- Jurić, M., Ivezić, Z., Brooks, A., et al. 2005, *astro-ph/0510520*
- Korchagin, V. I., Girard, T. M., Borkova, T. V., Dinescu, D. I., & van Altena, W. F. 2003, *AJ* 126, 2896
- Kroupa, P. 2002, *MNRAS*, 330, 707
- Larsen, J. A., & Humphreys, R. M. 2003, *ApJ*, 125, 1958
- Majewski, S. R. 1992, *ApJS*, 78, 87
- Majewski, S. R. 1993, *Ann. Rev. Astron. Astrophys.* 31, 575
- Majewski, S. R. 1994, in *Astronomy from wide-field imaging: proceedings of IAU Symp. 161*, ed. H. T. McGillivray, E. B. Thomson, B. M. Lasker, I. N. Reid, D. F. Malin, R. M. West & H. Lorenz (Dordrecht: Kluwer), 425
- Murray, C. A. 1986, *MNRAS*, 223, 649
- Norris, J. E. 1986, *ApJS*, 61, 667
- Norris, J. E. 1999, *Ap&SS*, 265, 213
- Ojha, D. K. 2001, *MNRAS*, 322, 426
- Parker, J. E., Humphreys, R. M., & Beers, T. C. 2004, *AJ*, 127, 1567
- Prohaska, J. X., Naumov, S.O., Carney, B. W., McWilliam, A., & Wolfe, A. M. 2000, *AJ*, 120, 2513
- Quinn, P. J., Hernquist, L., & Fullagar, D. P. 1993, *ApJ*, 403, 74
- Reid, N., & Majewski, S. R. 1993, *ApJ*, 409, 635
- Robin, A.C., Haywood, M., Creze, M., et al. 1996, *A&A*, 305, 125
- Rong, J., Buser, R., & Karaali, S. 2001, *A&A*, 365, 431
- Siegel, M. H., Majewski, S. R., Reid, I. N., & Thompson, I. B. 2002, *AJ*, 578, 151
- Soubiran, C., Bienaymé, O., & Siebert, A. 2003, *A&A*, 398, 141
- Toomre, A. 1962, *ApJ*, 138, 385

- Tsikoudi, V. 1979, ApJ, 234, 842
- Tsuchiya, T., Korchagin, V. I., & Dinescu, D. I. 2004, MNRAS, 350, 1141
- Velazquez, H. & White, S. D. M. 1999, MNRAS, 304, 254
- Wyse, R. F. G. & Gilmore, G. F. 1990, in *Chemical & Dynamical Evolution of Galaxies*, eds. F. Ferrini, J. Franco, F. Matteucci, p. 19, (Pisa:ETS Editrice)
- Wyse, R. F. G. & Gilmore, G. 1995, AJ 110, 2771
- Wyse, R. F. G., Gilmore, G. Norris, J. E., Wilkinson, M. I., Kleyna, J. T., Koch, A., Evans, N. W., & Grebel, E. K. 2006, ApJL, 639, 13
- Yi, S. K., Kim, Y.-C., & Demarque, P. 2003, ApJS 144, 259
- Yoachim, P. & Dalcanton, J. 2005, ApJ, 624, 701
- Yoachim, P. & Dalcanton, J. 2006, AJ, 131, 226
- Zinn, R. 1985, ApJ, 293, 424